





Human iPSC-Derived Microglia Sense and Dampen Hyperexcitability of Cortical Neurons Carrying the Epilepsy-Associated SCN2A-L1342P Mutation

Zhefu Que,^{1,2*} Maria I. Olivero-Acosta,^{1,2*} Morgan Robinson,^{1,2,3} Ian Chen,^{1,2}  Jingliang Zhang,^{1,2} Kyle Wettschurack,^{1,2} Jiaxiang Wu,^{1,2}  Tiange Xiao,^{1,2} Conrad Max Otterbacher,^{1,2} Vinayak Shankar,^{1,2} Hope Harlow,^{1,2} Seoyong Hong,^{1,2} Benjamin Zirkle,^{1,2} Muhan Wang,^{1,2} Ningren Cui,^{1,2} Purba Mandal,^{1,2} Xiaoling Chen,^{1,2} Brody Deming,^{1,2} Manasi Halurkar,^{1,2} Yuanrui Zhao,^{1,2} Jean-Christophe Rochet,^{1,2} Ranjie Xu,⁴ Amy L. Brewster,⁵  Long-jun Wu,⁶ Chongli Yuan,³ William C. Skarnes,⁷ and  Yang Yang^{1,2}

¹Borsch Department of Medicinal Chemistry and Molecular Pharmacology, College of Pharmacy, Purdue University, West Lafayette, Indiana 47907, ²Purdue Institute for Integrative Neuroscience (PIIN), Purdue University, West Lafayette, Indiana 47907, ³Department of Chemical Engineering, Purdue University, West Lafayette, Indiana 47907, ⁴Purdue University College of Veterinary Medicine, West Lafayette, Indiana 47907, ⁵Department of Biological Sciences, Southern Methodist University, Dallas, Texas 75205, ⁶Department of Neurology, Mayo Clinic, Rochester, Minnesota 55905, and ⁷The Jackson Laboratory for Genomic Medicine, Farmington, Connecticut 06032

Neuronal hyperexcitability is a hallmark of epilepsy. It has been recently shown in rodent models of seizures that microglia, the brain's resident immune cells, can respond to and modulate neuronal excitability. However, how human microglia interact with human neurons to regulate hyperexcitability mediated by an epilepsy-causing genetic mutation found in patients is unknown. The *SCN2A* gene is responsible for encoding the voltage-gated sodium channel Nav1.2, one of the leading contributors to monogenic epilepsies. Previously, we demonstrated that the recurring Nav1.2-L1342P mutation leads to hyperexcitability in a male donor (KOLF2.1) human-induced pluripotent stem cell (hiPSC)-derived cortical neuron model. Microglia originate from a different lineage (yolk sac) and are not naturally present in hiPSC-derived neuronal cultures. To study how microglia respond to neurons carrying a disease-causing mutation and influence neuronal excitability, we established a coculture model comprising hiPSC-derived neurons and microglia. We found that microglia display increased branch length and enhanced process-specific calcium signal when cocultured with Nav1.2-L1342P neurons. Moreover, the presence of microglia significantly lowered the repetitive action potential firing and current density of sodium channels in neurons carrying the mutation. Additionally, we showed that coculturing with microglia led to a reduction in sodium channel expression within the axon initial segment of Nav1.2-L1342P neurons. Furthermore, we demonstrated that Nav1.2-L1342P neurons release a higher amount of glutamate compared with control neurons. Our work thus reveals a critical role of human iPSC-derived microglia in sensing and dampening hyperexcitability mediated by an epilepsy-causing mutation.

Key words: channelopathy; electrophysiology; human-induced pluripotent stem cells (hiPSCs); hyperexcitability; monogenic diseases; seizures; voltage-gated sodium channel Nav1.2

Significance Statement

Seizure studies in mouse models have highlighted the role of microglia in modulating neuronal activity, particularly in the promotion or suppression of seizures. However, a gap persists in comprehending the influence of human microglia on intrinsically hyperexcitable neurons carrying epilepsy-associated pathogenic mutations. This research addresses this gap by investigating human microglia and their impact on neuronal functions. Our findings demonstrate that microglia exhibit dynamic morphological alterations and calcium fluctuations in the presence of neurons carrying an epilepsy-associated *SCN2A* mutation. Furthermore, microglia suppressed the excitability of hyperexcitable neurons, suggesting a potential beneficial role. This study underscores the role of microglia in the regulation of abnormal neuronal activity, providing insights into therapeutic strategies for neurological conditions associated with hyperexcitability.

Received Oct. 18, 2023; revised Oct. 16, 2024; accepted Nov. 8, 2024.

Author contributions: Z.Q., M.I.O.-A., and Y.Y. designed research; Z.Q., M.I.O.-A., M.R., I.C., J.Z., K.W., J.W., T.X., C.M.O., V.S., H.H., S.H., B.Z., M.W., N.C., P.M., X.C., B.D., M.H., and Y.Z. performed research; J.-C.R. and W.C.S. contributed unpublished reagents/analytic tools; M.I.O.-A., R.X., C.Y., A.L.B., and L.-j.W. analyzed data.

This work was supported by the National Institutes of Health (NIH)—National Institute of Neurological Disorders and Stroke (NINDS) Grants R01 NS117585 and R01 NS123154 (to Y.Y.). M.I.O.-A. is supported by the Fulbright-Coldenias Scholarship Program. This work was also supported, in part, by the Indiana Clinical and Translational Sciences Institute, by Award Number UL1TR002529 from the NIH, National Center for Advancing Translational Sciences, Clinical, and Translational Sciences Award. We thank Dr. Mark Estacion for his advice on the calcium imaging assay and electrophysiology.

We thank Dr. Shaoyou Chu from Indiana University for providing the pHrodo-Myelin. We also thank the support from the Purdue University Institute for Drug Discovery (PIDD) and the Purdue Institute for Integrative Neuroscience (PIIN). The Yang Lab thanks the *FamilieSCN2A* foundation for the Action Potential Award and the Hodgkin-Huxley Research Award.

*Z.Q. and M.I.O.-A. contributed equally to this work.

The authors declare no competing financial interests. ChatGPT was used to improve the readability and language of this work.

Correspondence should be addressed to Yang Yang at yangyang@purdue.edu.

<https://doi.org/10.1523/JNEUROSCI.12027-23.2024>

Copyright © 2024 the authors

Introduction

Epilepsy is a neurological disorder characterized by recurrent and spontaneous seizures (Christensen et al., 2023); when left uncontrolled, it can lead to neuronal damage (H. Sun et al., 2022), cognitive deficits (Chai et al., 2023), and even sudden unexpected death (Whitney et al., 2023). A prominent feature of epileptic seizures is hyperexcitability and excessive abnormal neural activity, which in some cases could be attributed to genetic changes in ion channels (Oyler et al., 2018). The *SCN2A* gene encodes the pore-forming sodium voltage-gated channel alpha subunit 2, an ion channel protein that mediates neuronal action potential (AP) firing. *SCN2A* pathogenic heterozygous mutations are monogenic causes of epilepsies (Wolff et al., 2017; Yokoi et al., 2018; Epifanio et al., 2021; Yang et al., 2022; Zeng et al., 2022). In fact, a recent study positions *SCN2A* as the third most prevalent gene harboring epilepsy-related mutations (Knowles et al., 2022). Among many *SCN2A* disease-causing mutations, the *de novo* heterozygous missense L1342P is a recurrent mutation associated with developmental and epileptic encephalopathy found in multiple patients worldwide (Wolff et al., 2017; Crawford et al., 2021).

Previously, we developed an *in vitro* disease model of seizures with monolayer (2D) cortical neurons derived from human-induced pluripotent stem cells (hiPSCs) carrying the epilepsy-associated Nav1.2-L1342P mutation. Our investigation revealed intrinsic and network neuronal hyperexcitability in the hiPSC-derived cortical neurons carrying this Nav1.2-L1342P mutation (Que et al., 2021). While neuronal hyperexcitability appears to be an intrinsic property of neurons carrying this *SCN2A* disease-causing mutation, emerging evidence suggests that non-neuronal cell types can influence neuronal excitability and thus can contribute to disease severity and progression (R. Chen et al., 2023). Microglia are brain-resident macrophages that originate from the yolk sac and migrate into the brain during development (Speicher et al., 2019). Mounting evidence suggests that microglia play a key role in regulating brain homeostasis and maintaining neural circuit integrity (Olson and Miller, 2004; Paolicelli et al., 2011; Schafer et al., 2012; McQuade et al., 2018; Weinhard et al., 2018). The impact of microglia on neuronal excitability has been extensively studied in rodents and found to be multifaceted and contingent upon the specific context. For instance, in certain cases, activated microglia release proinflammatory mediators that enhance neuronal activity, thereby promoting epileptogenesis (Henning et al., 2023). However, in other studies, microglia exert a regulatory role in limiting excessive neuronal activity, as observed in rodent models of chemically and genetically induced seizures (Eyo et al., 2014; Badimon et al., 2020; Merlini et al., 2021). While these published studies are vital for us to understand the microglia–neuron interactions, these studies rely on rodent models in which seizures and neuronal hyperexcitability are triggered by external chemicals (Eyo et al., 2014; Liu et al., 2020). No studies, however, have yet reported how human microglia respond to and regulate the excitability of intrinsically hyperexcitable human neurons carrying epilepsy-causing genetic mutations, hindering our understanding of microglia in human disease conditions.

In the current study, we utilized a coculture system of hiPSC-derived microglia and hiPSC-derived cortical neurons carrying the epilepsy-associated Nav1.2-L1342P mutation to study microglia–neuron interactions. We found an increase in the length of microglial branches when cocultured with Nav1.2-L1342P neurons. This effect paralleled an increase in calcium signaling within microglial processes. In addition, we demonstrated that hiPSC-derived microglia reduced hyperexcitability and sodium

current density in neurons carrying the Nav1.2-L1342P genetic mutation. Additionally, we demonstrated that coculture of neuron and microglia led to a reduction in sodium channel (Pan Nav) expression within the axon initial segment (AIS) of Nav1.2-L1342P neurons. Finally, we revealed that Nav1.2-L1342P neurons release a higher amount of glutamate, which may trigger the responses of microglia to regulate neuronal hyperexcitability. Taken together, our study illustrates the vital role of microglia in human epilepsy pathophysiology, suggesting a complex microglia–neuronal interaction with both cell types influencing each other's phenotypes.

Materials and Methods

Generation of hiPSC-derived cortical neurons. Previously described hiPSCs from a male donor expressing wild-type (WT; control) and CRISPR/Cas9-engineered Nav1.2-L1342P mutant channels (Que et al., 2021) were used in this study. Experiments were performed with four hiPSC lines (WT, KOLF2.1 and A03; L1342P, A12 and E09). Feeder-free hiPSCs colonies were grown on Matrigel (Corning, catalog #354230) and maintained in StemFlex (Thermo Fisher Scientific, catalog #A3349401) with daily media changes. Quality controls were performed for all lines, including Sanger sequencing, karyotyping, and immunocytochemistry. Undifferentiated hiPSC colonies displayed normal and homogenous morphology with defined edges and low levels of spontaneous differentiation. In addition, they consistently expressed standard pluripotency markers, including SOX2, TRA-1-80, OCT4, TRA-1-60, NANOG, and SSEA1 (data not shown).

A dual-SMAD inhibition method utilizing embryoid bodies (EBs) was used to generate cortical neurons based on our established protocol (Que et al., 2021). To generate EBs, hiPSC colonies were dissociated into single cells with Accutase (Innovative Cell Technologies, catalog #AT104) and seeded with 1× RevitaCell ROCK inhibitor supplement (Invitrogen, catalog #A2644501), for the initial 24 h on ultralow attachment 96-well plates (Corning, catalog #CLS3474-24EA) with a cell density of ~12,000 cells per microwell in an EB formation medium containing STEMdiff neural induction medium (STEMCELL Technologies, catalog #05835) supplemented with 100 nM of LDN-193189 (Sigma-Aldrich, catalog #SML0559) and 10 μM SB431542 (Tocris Bioscience, catalog #1614) to begin dual-SMADi neural induction. After 7 d, EBs were collected and seeded on Matrigel until the appearance of neural rosettes. A neural rosette selection reagent (STEMCELL Technologies, catalog #05832) was used to lift the rosette monolayer clusters, which were dissociated and seeded onto Matrigel-coated plates and cultured with dual-SMADi supplemented neural induction media, until the appearance of neural progenitor cells (NPCs). Stocks of NPC were expanded in STEMdiff neural progenitor media (STEMCELL Technologies, catalog #05833) frozen and stored for later differentiations.

Prior to seeding cells for differentiation, cultureware was coated with a 1:5 mixture of 0.01% poly-L-ornithine (PLO; Sigma-Aldrich, catalog #P4957) in phosphate-buffered saline (PBS) overnight at room temperature; subsequently, PLO-coated plates were incubated with 10 μg/ml mouse laminin (Corning, catalog #354232) in DMEM/F12 for 2 h at 37°C. To begin neural differentiation, we seeded neural progenitors onto PLO–laminin-coated vessels at a density of ~2.5 × 10⁴ cells/cm² and differentiated ~3 weeks in a media containing Neurobasal Plus medium (Invitrogen, catalog #A3582901), 1× NEAA solution (Invitrogen, catalog #11140050), 1× GlutaMAX (Invitrogen, catalog #3505006), PenStrep (10,000 U/ml; Invitrogen, catalog #15-140-163), 1× B27 plus supplement (Invitrogen, catalog #A3582801), 1× N2 supplement (Invitrogen, catalog #17-502-048), 100 μM dibutyryl cAMP (dcAMP; Santa Cruz Biotechnology, catalog #sc-201567A), 200 μM ascorbic acid (Wako Chemicals, catalog #323-44822), 20 ng/ml brain-derived neurotrophic factor (BDNF; Prospec Bio, catalog #CYT-207), and 20 ng/ml glial cell-derived neurotrophic factor (GDNF; Prospec Bio, catalog #CYT-305) with media replacement every 2–3 d. After 20 d, cells were replated at 1.5 × 10⁴ cells/cm² on glass coverslips coated with PLO–laminin using a complete maturation media formulation containing Neurobasal Plus

(Invitrogen, catalog #A3582901). After a week, the basal media were changed into Brainphys (STEMCELL Technologies, catalog #05790), PenStrep, 1× N2 supplement, 1× B27 plus supplemented with BDNF, GDNF, and cAMP in the same concentration previously described.

Generation of hiPSC-derived microglia. To produce hiPSC-derived microglia, we used two different control (WT) hiPSC lines, KOLF2.1 and GCaMP6f-H04. The KOLF2.1 cell line-derived microglia were cocultured with neurons for electrophysiology experiments. The GCaMP6f-H04 line has the GCaMP6f calcium indicator (T-W. Chen et al., 2013) engineered into the AAVS1 safe harbor locus of the reference Kolf2.1 iPSC line using CRISPR/Cas9-mediated knock-in and was used for the microglial calcium imaging. Specifically, a commercially available plasmid (pAAVS1-PC-GCaMP6f, plasmid #73503) containing the GCaMP6f knock-in construct was used to generate the GCaMP6f-H04 line from KOLF2.1 reference iPSCs line. For each experiment, at least two differentiations (biological replicates) were performed for each cell line.

To begin microglia differentiation, we largely followed a commercially available kit based on well-established, previously published protocols (Abud et al., 2017; McQuade et al., 2018; McQuade and Blurton-Jones, 2021). Briefly, feeder-free hiPSCs were grown and maintained on Matrigel, guided toward a mesodermal, hematopoietic lineage to obtain hematopoietic progenitor cells (HPCs) using the STEMdiff Hematopoietic Kit (STEMCELL Technologies, catalog #05310). Next, HPCs were converted into homeostatic microglia on cultureware coated with Matrigel in differentiation medium composed of DMEM/F12 basal media (Invitrogen, catalog #11-320-033); 2× 100× Insulin–Transferrin–Selenium (ITS-G; Invitrogen, catalog #41400045); 2× B27, 0.5× N2, 1× GlutaMAX (Invitrogen, catalog #35050061); 1× nonessential amino acids (Invitrogen, catalog #11140050), 400 μM monothio glycerol (Sigma-Aldrich, catalog #M6145-25ML), and 5 μg/ml insulin (Sigma-Aldrich, catalog #12643-25MG). Before use, this medium was supplemented with 25 ng/ml cytokine macrophage colony-stimulating factor 1 (Sigma-Aldrich, catalog #300-25), 100 ng/ml interleukin-34 (PeproTech, catalog #200-34), and 50 ng/ml transforming growth factor beta 1 (PeproTech, catalog #100-21) until Day 24. Then, cells were cultured in a maturation medium with the same composition as the differentiation medium, with the addition of 100 ng/ml of cluster of differentiation 200/OX-2 membrane glycoprotein (ACROBiosystems, catalog #50-101-8369) and 100 ng/ml of CX3CL1 (fractalkine/chemokine (C-X3-C motif) ligand 1; PeproTech, catalog #300-31) for up to 12 d.

Coculture of hiPSC-derived microglia and hiPSC-derived cortical neurons. We established a coculture model to study the interaction of neurons and microglia, as microglia developmentally come from the yolk sac and thus do not naturally exist in hiPSC-derived neuronal culture. Initially, hiPSC-derived cortical neurons and microglia were generated and maintained separately as above. To generate the coculture, we replated cortical neurons derived from hiPSCs, which had been differentiated for 38 d, at a density of 10,000 cells per well in a 96-well clear-bottom plate previously coated with PLO–laminin as above. The next day, microglia derived from hiPSCs matured for 31 d were seeded directly on top of the previously seeded cortical neuron monolayers, at a 1:1 seeding ratio between microglia and neurons, which was used in published studies (Haenseler et al., 2017; Vahsen et al., 2022). For medium exchange, a mixture of half-complete neurobasal medium and half microglia maturation medium was used, with media exchanges performed every 2 d. The coculture was maintained for a total of 7 d to allow for the formation of interactions between the two cell types before assays were performed.

Immunocytochemistry. hiPSC-derived microglia cells were cultured on glass coverslips (Neuvitro, catalog #GG-12-Pre) or 24-well glass-bottom plates with number 1.5 cover glass (Celvis, catalog #P24-1.5H-N) previously coated with a PLO–laminin as above. Before the experiment, the samples were briefly washed in PBS (Corning, catalog #21-040-CMX12) and then fixed in 4% paraformaldehyde in PBS at room temperature (RT) for 15 min. Following fixation, the samples were rinsed three times with PBS (5 min per rinse) and permeabilized with 0.3% Triton X-100, pH 7.4, surfactant for 20 min.

The fixed and permeabilized hiPSC-derived microglia were treated with 5% bovine serum albumin (BSA; Sigma-Aldrich, catalog #9048) to block nonspecific binding for 1 h at RT. Subsequently, the samples were incubated overnight at 4°C in a humidified chamber with primary antibodies diluted in 1% BSA. The primary antibodies used included rabbit anti-P2RY12 (purinergic receptor P2Y12; Sigma Prestige Antibodies, catalog #HPA014515), rabbit anti-TMEM119 (transmembrane protein 119; Sigma Prestige Antibodies, catalog #HPA051870), and rabbit anti-IBA1 (ionized calcium-binding adaptor molecule 1; Abcam, catalog #178846). The following day, the samples were rinsed three times with PBS and then incubated with fluorescent dye-conjugated secondary antibodies, which were diluted in 1% BSA for 2 h at RT in the dark. After the incubation, the secondary antibody solution was removed, and the coverslips were washed three times with PBS (5 min per wash) in the dark.

For staining hiPSC-derived neurons, primary antibodies for mouse anti-MAP2 (microtubule-associated protein 2; Invitrogen, catalog #13-1500, 1:1,000) and guinea pig anti-synapsin1/2 (SYN1/2; Synaptic Systems, catalog #106044, 1:1,000) were used. Microglial images were acquired with a Nikon Ti2 Eclipse fluorescence microscope, while images of the microglia–neuron coculture were captured using a ZEISS LSM 900 confocal microscope.

For AIS and Pan Nav immunocytochemistry, slight modifications of the previous staining protocol were made. Briefly, 2% PFA fixative was used for 15 min. Block and permeabilization were done concurrently with 5% BSA and 0.3% Triton X-100 solution. The primary antibodies for mouse anti-ankyrin-G (ANK-G; Antibodies, catalog #75-146, 1:200) and rabbit anti-Pan Nav (Alomone Labs, catalog #ASC-003, 1:200) were used. Somatodendritic marker for chicken anti-MAP2 (Novus Biologicals, catalog #NB300-213, 1:500) was used to locate neuron morphology. Images were acquired with a Zeiss LSM 900 confocal microscope with a 63× Plan Apo Oil objective. Quantification of the AIS was performed by manually tracing the morphology of the AIS using the Zen Blue software. Parameters obtained included length and signal intensity of Pan Nav within the AIS.

The secondary antibodies used for fluorescently labeling hiPSC-derived neurons and microglia were as follows: anti-rabbit antibodies conjugated with Alexa Fluor 488 (Invitrogen, catalog #A11008 1:1,000) or anti-mouse antibodies conjugated with Alexa Fluor 488 (Invitrogen, catalog #A11001 1:1,000), anti-rabbit antibodies conjugated with Alexa Fluor 555 (Invitrogen, catalog #A32732, 1:1,000) or anti-mouse antibodies conjugated with Alexa Fluor 555 (Invitrogen, catalog #A32727, 1:1,000), anti-guinea pig antibodies conjugated with Alexa Fluor 488 (Invitrogen, catalog #A11073, 1:1,000), and anti-chicken antibodies conjugated with Alexa Fluor 647 (Invitrogen, catalog #A32933 1:1,000). For DAPI counterstaining, either VECTASHIELD Antifade Mounting medium with DAPI (Vector Laboratories, catalog #H-1200) or a PBS-DAPI solution (Thermo Fisher Scientific, catalog #62238, 1:10,000) was used.

IncuCyte SX5 live-cell phagocytotic assay. To assess the phagocytic activity of microglia derived from hiPSCs, we used pHrodo-Myelin, a pH-sensitive dye combined with a myelin fragment (Hendrickx et al., 2014), graciously provided by Dr. Shaoyou Chu from Indiana University (Mason et al., 2023). First, we prepared a Corning number 1.5 glass-bottom 96 well by coating it with a 20 μg/ml diluted solution of poly-D-lysine in 1× PBS, letting it incubate at 37°C overnight. Subsequently, the wells were washed three times with 1× PBS. Approximately 15,000 matured hiPSC-derived microglia cells, suspended in 100 μl of microglia maturation media, were placed delicately onto the coated wells. The plate was then left in an incubator at 37°C overnight. The following day, we prepared a stock of pHrodo-myelin at 5 μg/ml in the microglia maturation media. The medium of 50 μl was extracted from each well, and 50 μl of the pHrodo-myelin stock was added, resulting in a final concentration of 2.5 μg/ml of pHrodo-myelin. To monitor the uptake of the pHrodo-myelin dye for 48 h, we employed an IncuCyte SX5 imaging system with an orange filter and bright field using a 20× objective. The exposure time was maintained at 300 ms. To quantify the phagocytic activity, we calculated the normalized integrated intensity of pHrodo-myelin by dividing the total integrated intensity of pHrodo-myelin corresponding to each well over the area occupied by the microglial cells, as identified by the bright-field channel.

Morphological characterization of hiPSC-derived IBA1+ microglia. To assess alterations in microglia morphology following coculture with control (WT) and Nav1.2-L1342P cortical neurons, we conducted immunocytochemistry staining for microglia-specific marker IBA1. The ImageJ Analyze Skeleton plugin (available at <https://imagej.net/plugins/analyze-skeleton/>) was employed to generate a skeletonized representation of microglial morphology, which was used to determine the unique average length of the microglial processes per field of view (Jairaman et al., 2022). To obtain area, circularity, and perimeter measurements, we manually selected clearly defined microglial morphologies using the Nikon Imaging Software-Elements (NIS-Elements) region of interest (ROI) editor and used the automatic measurement results to obtain values. We measured between 7 and 35 microglia per field of view.

Live-cell calcium imaging of hiPSC-derived microglia expressing GCaMP6. Live-cell calcium imaging was conducted using an inverted widefield Nikon Eclipse Ti2 microscope. Time-lapse recordings were acquired at a frequency of 1 Hz for 200 s. Microglial somata and processes were manually defined using Fiji's ImageJ (Version 2.3.0/1.53f; Schindelin et al., 2012) software's ROI editor. Time measurements were performed to detect the spontaneous calcium transient fluctuations. The signal intensity was normalized as $\Delta F/F$, where ΔF represents the difference between an individual ROI's fluorescence intensity (F) and its minimum intensity value (F_{\min}). The normalized data were then transferred to OriginPro (Origin2021b version 9.8.5.201) for peak detection and quantifications. We used the NIS-Elements (Version 5.02) for representative image processing.

Electrophysiology of hiPSC-derived neurons cocultured with hiPSC-derived microglia. Whole-cell patch-clamp recordings were made using an EPC10 amplifier and Patchmaster v2X90.3 software (HEKA Elektronik) paired to an inverted microscope configuration (NikonTi-2 Eclipse). The recording was performed at RT. For the current-clamp recording, the external solution contained the following (in mM): 140 NaCl, 5 KCl, 2 CaCl₂, 2 MgCl₂, 10 HEPES, and 10 dextrose, titrated with NaOH to pH 7.3. The internal solution contained the following (in mM): 128 K-gluconate, 5 KCl, 5 NaCl, 1 MgCl₂, 3 Mg-ATP, 1 EGTA, 10 HEPES, and 10 dextrose, titrated with KOH to pH 7.2. The osmolality was brought to 320 and 310 mOsm by adding dextrose for the extracellular and internal solutions, respectively. For current-clamp recording, the glass pipettes (BF150-86-10) were used and pulled to reach the resistances of 4–8 M Ω . We measured the repetitive AP firings at increased current injections using a prolonged 800 ms present stimulus ranging from 0 to 125 pA in 5 pA increments. Neurons were transfected with the AAV-CamKII-GFP virus (Addgene 50469-AAV9), and neurons with GFP-positive signals were selected for patch-clamp experiments.

For experiments under the voltage-clamp configuration, we used our previously reported patch solution and protocol (Que et al., 2021). Thick-wall borosilicate glass pipettes (BF150-86-10) were pulled to reach the resistances of 2–4 M Ω . Briefly, the activation curve from the voltage-gated sodium channel was achieved by 10 ms steps from -70 to $+50$ mV in a 5 mV increment, with a holding potential of -100 mV. The currents from both groups were recorded at 5 min after obtaining the whole-cell configuration. P/N leak subtraction procedure was applied during the protocol. At least 70% of the series resistance was compensated. The current density was obtained by normalizing the current amplitude to the capacitance under each corresponding voltage. To calculate G_{\max} and the normalized G/G_{\max} - V curve, the I - V trace was fitted with a Boltzmann I - V curve fit (OriginPro) to obtain the reversal potential (V_{rev}), followed by the sodium conductance, calculated as $G = I_p / (V - V_{\text{rev}})$, where I_p was the peak current amplitude (relative to the holding potential) under each voltage step (V_m ; Que et al., 2021). The Boltzmann I - V curve fit at high polarization levels (above $+45$ mV) are subject to significantly high variability, consequently these data points were excluded prior to curve fitting.

Extracellular glutamate assay of hiPSC-derived neurons. To measure the glutamate release from WT and Nav1.2-L1342P neurons, we used a bioluminescence-based assay (Glutamate-Glo, Promega, catalog #J7021) for detection of glutamate in biological samples. Initially, cultures of WT

and Nav1.2-L1342P hiPSC-derived neurons in 24-well plates were placed at equal densities. A standard media change was performed, and 2 d later (~ 48 h), we collected the conditioned culture media from the wells to measure glutamate levels. This medium was then mixed with a glutamate detection reagent in a 1:1 ratio following the manufacturer's instructions. Mixed medium was then added to a 384-well white flat-bottom plate (Thermo Fisher Scientific, catalog #12-565-343), centrifuged for 5 min at $300 \times g$, and incubated for 2 h at RT prior to luminescence detection. Total luminescence was measured with a Synergy H1 plate reader with the gain set to 200.

Statistical analysis. GraphPad Prism (version 9.5.1) and OriginPro 2021b (version 9.8.5.201) were used for statistical analysis. The number of experimental samples (n) in each group was indicated in the figure legend. Results are presented as mean \pm standard error of the mean (SEM). Values are shown in figures as * $p < 0.05$, ** $p < 0.01$, *** $p < 0.001$, and **** $p < 0.0001$ and n.s. (not significant) as $p \geq 0.05$. The detailed statistical methods are described in the relevant results sections.

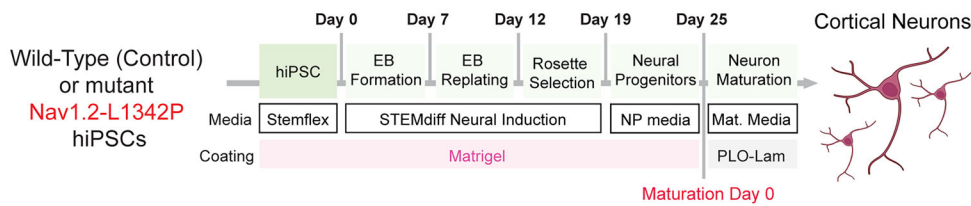
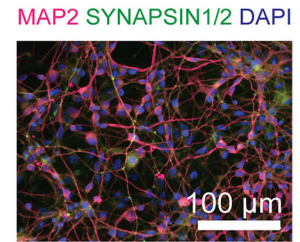
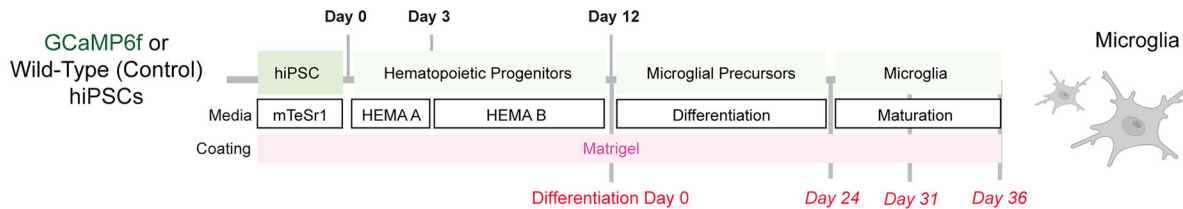
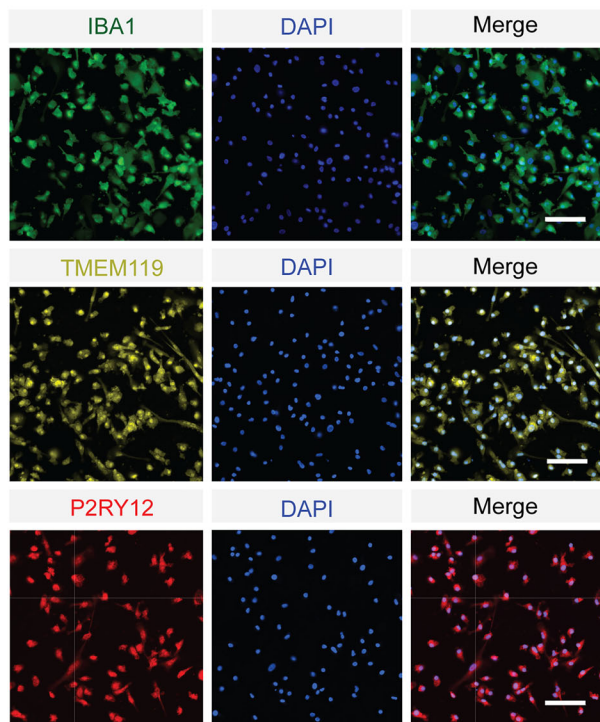
Results

hiPSC-derived microglia express relevant markers and display phagocytotic capacity

While microglia play an indispensable role in the brain, they developmentally originate from the yolk sac and thus do not naturally appear in hiPSC-derived neuronal culture (Lukens and Eyo, 2022); therefore, a coculture model of neurons and microglia needs to be established to study the interaction between these cells. To this end, neurons and microglia were differentiated using distinct protocols and characterized, before being cultured together. To generate glutamatergic cortical neurons, we differentiated hiPSCs using our published protocol (Que et al., 2021; Fig. 1A), which can yield electrically active neurons after 45 d of maturation in vitro (post-NPC stage). These neurons express synaptic and neuron-specific markers such as SYN1/2 and MAP2 (Fig. 1B). Since Nav1.2 is minimally expressed in microglia from mice and hiPSC-derived microglia (Black et al., 2009; Black and Waxman, 2012, 2013; Abud et al., 2017; Grubman et al., 2020; Dräger et al., 2022), we intentionally used microglia derived from control reference (WT) hiPSC lines to simplify the research design. Control (WT) mature microglia were generated after 24 d of differentiation (Fig. 1C) and were characterized via staining and quantification of microglia-specific markers, including IBA1, TMEM119, and P2RY12 (Fig. 1D). We observed a high percentage of microglial cells after differentiation ($98.43 \pm 0.44\%$ TMEM119 labeling; $n = 18$ fields of view; two differentiations; $97.18 \pm 1.44\%$ IBA1 labeling; $n = 13$ fields of view; two differentiations; and $93.59 \pm 0.45\%$ of P2RY12 labeling; $n = 19$ fields of view; two differentiations). Our results thus indicate that hiPSC-derived microglia can be successfully obtained in a relatively homogeneous population. Next, we investigated the phagocytic function of the differentiated microglia. As immune and professional phagocyte cells, microglia can engulf substrates like synaptic and myelin debris. To evaluate the phagocytic capacity of the mature microglia, we exposed them to pHrodo-labeled myelin particles. Over 36 h, we observed the continuous internalization of myelin by the microglia, an ability that was also demonstrated in primary human microglia (Hendrickx et al., 2014), indicating their robust phagocytic ability (Fig. 1E).

Microglia cocultured with Nav1.2-L1342P cortical neurons display morphological alterations

In response to seizures, microglia extend and retract their extended processes to survey the brain and regulate network hyperexcitability (Merlini et al., 2021). However, how human microglia respond

A Generation of hiPSC-derived cortical neurons**B** hiPSC-derived neurons**C** Generation of hiPSC-derived microglia**D** Microglia Characterization

Quantification

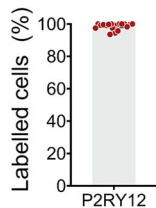
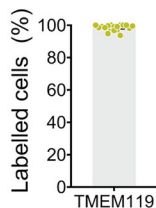
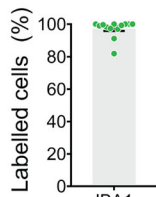
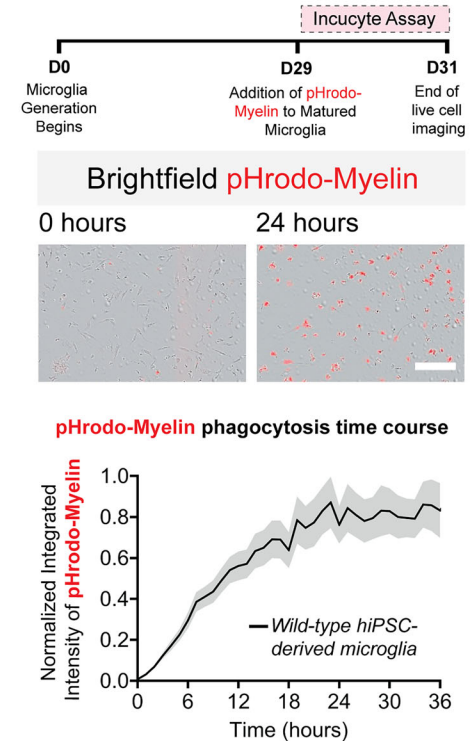
**E** Phagocytosis Assay

Figure 1. Characterization of hiPSC-derived cortical neurons and microglia. **A**, Schematic illustrating the protocol for generating hiPSC-derived cortical neurons. **B**, Representative fluorescent image of hiPSC-derived neurons stained for somatodendritic marker MAP2 (magenta), synaptic vesicle proteins SYN1/2 (green), and DAPI (blue). **C**, Schematic illustrating the protocol for generating hiPSC-derived microglia. hiPSCs are differentiated into HPCs for 12 d and cultured in microglia differentiation media for 24 d. The microglia maturation process is then carried out for up to 12 d. **D**, Representative images of hiPSC-differentiated microglia expressing microglial-specific markers: IBA1 (**D**, top panel, green, $n = 13$ fields of view, two differentiations), TMEM119 (**D**, middle panel, yellow, $n = 18$ fields of view, two differentiations), P2RY12 (**D**, lower panel red, $n = 19$ fields of view, two differentiations). DAPI was used to stain nuclei. Data are presented as mean \pm SEM. Scale bar, 100 μ m. **E**, Phagocytosis of pHrodo-myelin by WT (control) hiPSC-derived microglia. Data were obtained from one differentiation of three wells (48 images per well). Representative images at 0 and 24 h after the addition of pHrodo-myelin. hiPSC-derived microglia phagocytosed the pHrodo-labeled bioparticles, showing a gradually increasing red fluorescent signal over time. Scale bar, 25 μ m. hiPSC, human-induced pluripotent stem cells; EB, embryoid body; NP, neural progenitors; MAP2, microtubule-associated protein 2; SYN1/2, synapsin1/2; IBA1, ionized calcium-binding adaptor molecule 1; TMEM119, transmembrane protein 119; P2RY12, purinergic receptor P2Y12.

to human neurons carrying seizure-related genetic mutations is not known. Thus, we sought to investigate whether hiPSC-derived microglia would exhibit morphological changes when cocultured with hiPSC-derived hyperexcitable neurons carrying a Nav1.2-L1342P mutation (Que et al., 2021). To achieve this, we conducted a coculture experiment by seeding the microglia on top of neuronal monolayers and maintaining them for 7 d, as

illustrated in Figure 2A. We confirmed the presence of microglia and neurons in the cocultures with IBA1 (microglia, red) and MAP2 (neurons, green) by immunocytochemistry (Fig. 2B).

To evaluate microglia morphology, we manually traced the IBA1-positive microglial processes in coculture with hiPSC-derived cortical neurons (Fig. 2C,D). Our results revealed that microglia exhibited a significant increase in process length per cell when

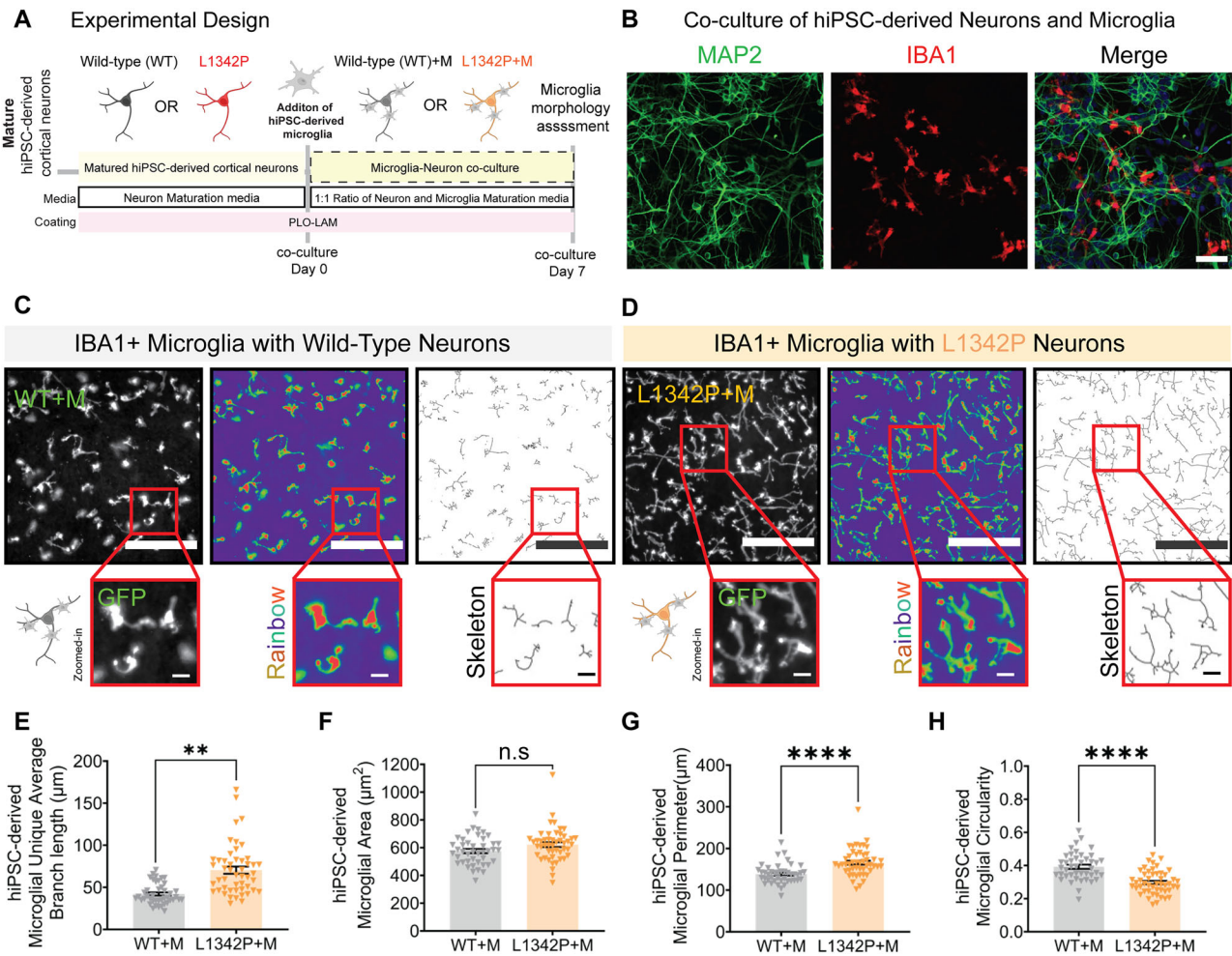


Figure 2. Human microglia in coculture with Nav1.2-L1342P neurons display morphological changes. **A**, The hiPSC-derived neurons and microglia were matured separately, and then microglia were seeded on top of neurons for 7 d before imaging. **B**, Representative images of cocultured neurons stained for neuron-specific marker MAP2 (green), microglia stained for IBA1 (red), and DAPI (blue) as a nuclear stain. **C, D**, hiPSC-derived microglia in coculture with control (WT) neurons (WT + M, **C**) and Nav1.2-L1342P neurons (L1342P + M, **D**). IBA1+ microglia cocultured with the hyperexcitable Nav1.2-L1342P neurons displayed an extended ramified process compared with coculture with control (WT) neurons. Images are pseudocolored in a rainbow gradient to facilitate identification, and the skeletonized view was included to detail branches. **E**, The microglial average branch length increases in coculture with Nav1.2-L1342P cortical neurons (WT + M, $n = 43$ fields of view, and L1342 + M, $n = 49$ fields of view; three differentiations; two clones per condition). **F**, The total microglial area shows a trend toward being increased in coculture with Nav1.2-L1342P neurons (WT + M, $n = 43$ fields of view, and L1342 + M, $n = 49$ fields of view; three differentiations; two clones per condition). **G**, Microglial perimeter is enhanced in coculture with Nav1.2-L1342P neurons, indicating extended processes (WT + M, $n = 43$ fields of view, and L1342 + M, $n = 49$ fields of view; three differentiations; two clones per condition). **H**, Microglial circularity is decreased in coculture with Nav1.2-L1342P neurons, indicating that they are less amoeboid-like (WT + M, $n = 43$ fields of view, and L1342 + M, $n = 49$ fields of view; three differentiations; two clones per condition). Each dot represents the mean value of a parameter per field of view. Data are presented as mean \pm SEM. Scale bar, 50 μm . Data were pooled from three differentiations. Data were analyzed by nested t test; ** $p < 0.01$ and **** $p < 0.0001$.

cocultured with the Nav1.2-L1342P mutant neurons versus when cocultured with control (WT) neurons (WT + M, $42.08 \pm 1.89 \mu\text{m}$; $n = 43$ fields of view; L1342P + M, $70.40 \pm 4.27 \mu\text{m}$; $n = 49$ fields of view; three differentiations; two clones per condition; nested t test; ** $p < 0.01$; Fig. 2E). In terms of total microglial area (soma and processes), we found no significant alterations in either coculture, indicating there were no changes in microglial cell size (WT + M, $575.30 \pm 15.30 \mu\text{m}^2$; $n = 43$ fields of view; L1342P + M, $621.50 \pm 17.21 \mu\text{m}^2$; $n = 49$ fields of view; three differentiations; two clones per condition; nested t test; n.s.; Fig. 2F). However, the microglial perimeter was increased in microglia cocultured with the Nav1.2-L1342P cortical neurons. Considering microglia size did not change, these data thus could be interpreted as microglial processes, such as extensions and branches, were increased (WT + M, $138.50 \pm 3.56 \mu\text{m}$; $n = 43$ fields of view; L1342P + M, $166.00 \pm 4.67 \mu\text{m}$; $n = 49$ fields of view; three differentiations; two clones per condition; nested t test; **** $p < 0.0001$; Fig. 2G). Microglia

circularity was also calculated with the circularity index expressed between 0 and 1 (1 representing a perfect circle), calculated as $4\pi A/P^2$, where A is the area and P is the perimeter. We found that the microglia circularity index was also decreased when cocultured with the Nav1.2-L1342P neurons (WT + M, 0.3924 ± 0.01 ; $n = 43$ fields of view; L1342P + M, 0.30 ± 0.01 ; $n = 49$ fields of view; three differentiations; two clones per condition; **** $p < 0.0001$; nested t test; Fig. 2H). Taken together, our data showed that microglia cocultured with mutant Nav1.2-L1342P neurons display increased process length compared with microglia cocultured with control (WT) neurons, revealing that hyperexcitable neurons influence the morphology of microglia.

Calcium signaling in hiPSC-derived microglia is enhanced when cocultured with L1342P neurons

Previous work using in vivo mouse models indicated that microglial calcium signals could respond to chemically triggered

neuronal activity changes (Umpierre et al., 2020). However, how human microglia sense and respond to intrinsically hyperexcitable human neurons carrying an epilepsy mutation remains to be elucidated. Thus, we carried out experiments to address this gap. To study the calcium dynamics of our hiPSC-derived microglia, we established a hiPSC line in which the endogenous AAVS1 safe harbor site was engineered with GCaMP6f using CRISPR/Cas9. We differentiated the GCaMP6f-iPSC lines into microglia and cocultured them with hiPSC-derived cortical neurons. Our results demonstrated that GCaMP6f-hiPSC-derived microglia in coculture with either WT neurons or neurons carrying Nav1.2-L1342P mutation can display spontaneous Ca²⁺ activity, reflected in continuously changing GCaMP6f calcium signal fluctuations (Fig. 3A,B). This assay thus allows us to determine how calcium dynamics in microglia respond to neurons with different excitability.

Microglia are made up of microdomains (soma and extended processes) that can have different calcium signaling patterns (Umpierre et al., 2020). Therefore, we divided calcium fluctuation measurements into three categories: (1) entire (global) microglial calcium activity and compartmentalized activity within (2) soma and (3) processes. We first analyzed the calcium activity patterns

from the entire microglia compartment. We found that the spikes generated from microglia in coculture with Nav1.2-L1342P neurons had a larger amplitude than those microglia in coculture with control (WT) neurons when the measurement was done for the entire microglia area. Specifically, we observed an elevated calcium signal, measured using the area under the curve (AUC), in microglia cocultured with Nav1.2-L1342P neurons, which was almost twice that of the WT (WT + M, 0.652 ± 0.045; n = 209 cells; L1342P + M, 1.125 ± 0.086; n = 168 cells; ****p < 0.0001; Mann-Whitney U test; Fig. 3C). Additionally, we observed that the average microglial spike amplitude increased more than twofold when cocultured with Nav1.2-L1342P neuron (WT + M, 0.069 ± 0.004; n = 204 cells; L1342P + M, 0.168 ± 0.012; n = 168 cells; ****p < 0.0001; Mann-Whitney U test; Fig. 3D).

When analyzing the calcium dynamics of separate microglial subcompartments, we found no significant difference in the average calcium signal AUC for the soma (average AUC for soma; WT + M, 1.238 ± 0.066; n = 100 cells; L1342P + M, 1.494 ± 0.175; n = 92 cells; n.s., p = 0.987; Mann-Whitney U test; Fig. 3E). There was also no significant difference in the average microglial spike amplitude per soma between microglia cocultured with either WT neurons or Nav1.2-L1342P neurons (average

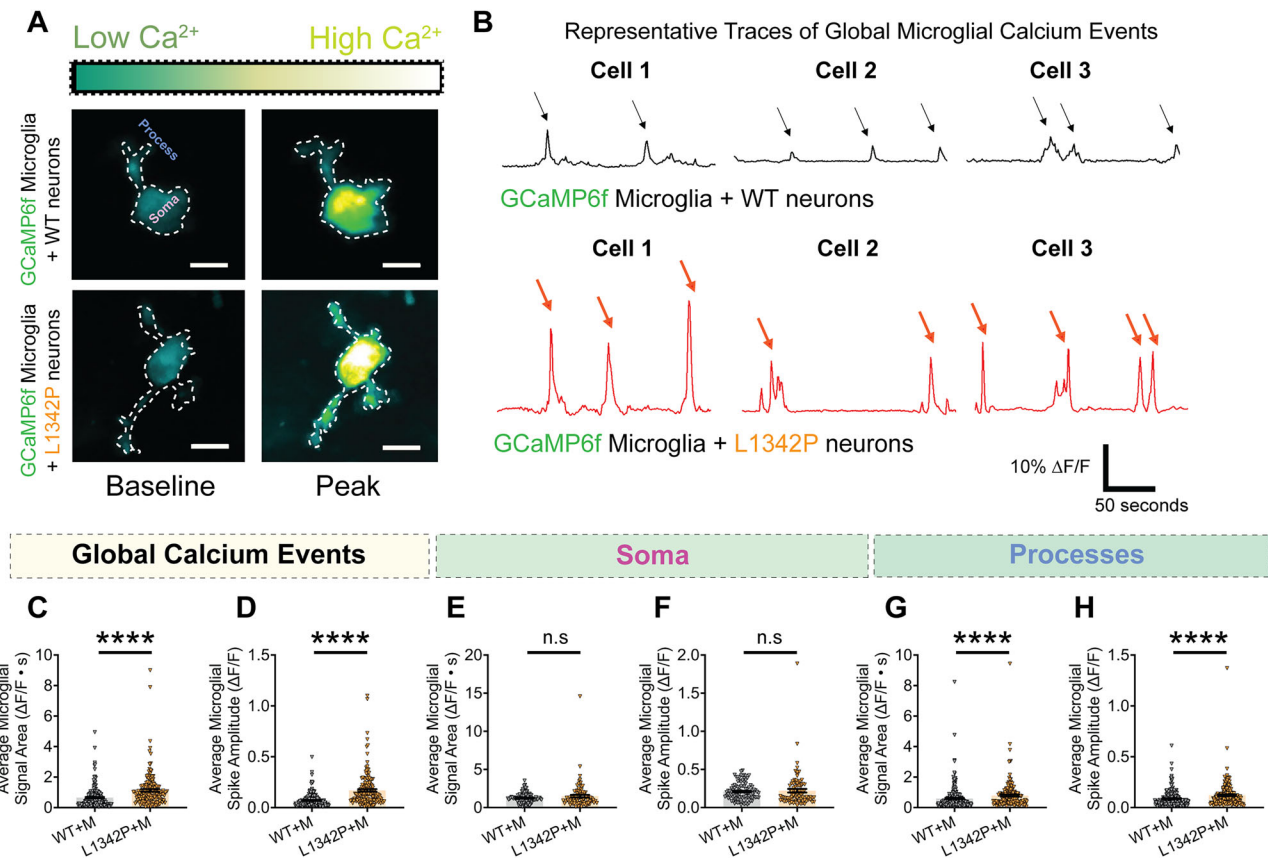


Figure 3. Calcium signal is enhanced in human microglia processes when cocultured with hyperexcitable hiPSC-derived Nav1.2-L1342P neurons. **A**, Fluorescent images of hiPSC-derived microglia expressing GCaMP6f cocultured with WT (top) and mutant Nav1.2-L1342P (bottom) hiPSC-derived neurons. The calcium signal is pseudocolored, with dark green indicating low signal and yellow hues depicting high signal. **B**, Representative ΔF/F traces of global calcium activity of microglia in coculture with control (WT) neurons (top, black) or Nav1.2-L1342P neurons (bottom, red). Three representative cells per condition are shown. **C**, The global average microglia calcium signal area increases in coculture with Nav1.2-L1342P neurons (WT + M, n = 209 cells, and L1342P + M, n = 168 cells). **D**, The global average microglial calcium spike amplitude increases in coculture with Nav1.2-L1342P neurons (WT + M, n = 204 cells, and L1342P + M, n = 168 cells). **E**, The average microglial signal area in the soma microdomain is not statistically different in the two coculture conditions (WT + M, n = 100 cells; L1342P + M, n = 92 cells). **F**, The average microglial spike amplitude in the soma microdomain is not statistically different in the two coculture conditions (WT + M, n = 100 cells; L1342P + M, n = 92 cells). **G**, The average microglial calcium signal area of the processes microdomain is increased in coculture with Nav1.2-L1342P neurons (WT + M, n = 250 processes; L1342P + M, n = 183 processes). **H**, The processes' average microglial calcium spike amplitude increases in coculture with L1342P neurons (WT + M, n = 250 processes; L1342P + M, n = 183 processes). Data were collected from three coverslips from two independent differentiations. Data in C–H were analyzed with Mann-Whitney's U test. ****p < 0.0001 and n.s. (not significant).

microglial spike amplitude per soma; WT + M, 0.211 ± 0.011 ; $n = 100$ cells; L1342P + M, 0.221 ± 0.023 ; $n = 92$ cells; n.s., $p = 0.281$; Mann–Whitney U test; Fig. 3F). On the other hand, we found that the average calcium signal AUC for the process was significantly higher in microglia cocultured with Nav1.2-L1342P neurons compared with these in microglia cocultured with control (WT) neurons (average AUC for microglial processes; WT + M, 0.595 ± 0.047 ; $n = 250$ processes; L1342P + M, 0.786 ± 0.067 ; $n = 183$ processes; **** $p < 0.0001$; Mann–Whitney U test; Fig. 3G). Moreover, the average microglial spike amplitude per process was enhanced in microglia cocultured with Nav1.2-L1342P neurons (average microglial spike amplitude per process; WT + M, 0.087 ± 0.005 ; $n = 250$ processes; L1342P + M, 0.121 ± 0.009 ; $n = 183$ processes; **** $p < 0.0001$; Mann–Whitney U test; Fig. 3H). Our human cell results suggest that hyperexcitable neurons trigger increased calcium signaling within the microglial process but may not be sufficient to alter calcium activity in the microglial soma, similar to the phenomena previously described in mice (Umpierre et al., 2020).

The repetitive firing of hiPSC-derived neurons carrying the Nav1.2-L1342P is reduced with microglia coculture

Altered microglia morphology and calcium signal indicated that microglia could respond to intrinsically hyperexcitable neurons carrying the disease-causing Nav1.2-L1342P genetic mutations. Thus, we investigated whether human microglia could concurrently affect the excitability of these neurons. To this end, we performed a whole-cell current-clamp to study the repetitive firing of WT and Nav1.2-L1342P cortical neurons with or without microglia in the culture. To visualize the excitatory neuronal populations, we transduced the neurons with pAAV-CaMKIIa-eGFP, enabling fluorescent detection of excitatory neurons for patch-clamp recording. Subsequently, we seeded microglia on top of the neurons, creating a coculture system as before. The coculture was maintained for 7 d, allowing for the establishment of proper interactions between microglia and neurons (Fig. 4A).

Representative AP firing traces show that WT neurons alone (Fig. 4B, left panel) and in coculture with microglia (Fig. 4B, right panel) exhibited no significant change in their AP firing trends. Quantitatively, the AP firing of control (WT) neurons cocultured with microglia did not significantly differ from control (WT) neurons alone (repeated-measure two-way ANOVA; $F_{(1,28)} = 0.532$; n.s., $p = 0.472$; WT, $n = 12$ neurons; two differentiations; WT + M, $n = 18$ neurons; two differentiations; Fig. 4D). However, a distinct finding emerged when using the Nav1.2-L1342P neurons. In isolation, the Nav1.2-L1342P neurons (Fig. 4C, left panel) displayed extensive APs firing at higher current injections, consistent with our previous work (Que et al., 2021). Notably, when cocultured with microglia, the Nav1.2-L1342P neurons exhibited reduced firing (Fig. 4C, right panel), indicating that microglia could modulate the neuronal activity of hyperexcitable Nav1.2-L1342P neurons. Quantitatively, the Nav1.2-L1342P neurons cocultured with microglia fired significantly fewer APs than Nav1.2-L1342P neurons alone (repeated-measure two-way ANOVA; $F_{(1,37)} = 6.421$; * $p = 0.016$; L1342P, $n = 14$ neurons; two differentiations; L1342P + M, $n = 25$ neurons; two differentiations; Fig. 4E).

Additionally, we observed that the AUC of the AP number versus current injection plots remained unchanged in the WT and WT + M comparison (WT, 522.3 ± 77.8 ; $n = 12$ neurons; two differentiations; WT + M, 535.0 ± 55.15 ; $n = 18$ neurons; two differentiations; two-way ANOVA with Tukey's multiple comparisons; n.s., $p = 0.9994$; Fig. 4F). In contrast, the AUC

was significantly reduced in the L1342P + M conditions compared with L1342P neurons (L1342P, 915.1 ± 97.46 ; $n = 14$ neurons; L1342P + M, 628.9 ± 58.85 ; $n = 24$ neurons; two-way ANOVA with Tukey's multiple comparisons; * $p = 0.0091$; Fig. 4F). This finding indicates that the presence of microglia specifically diminishes the AP responsiveness in mutant hiPSC-derived neurons. We also compared WT and L1342P neurons in the absence of microglia, and the AUC was increased in the L1342P compared with the control (WT, 522.3 ± 77.8 ; $n = 12$ neurons; two differentiations; L1342P, 915.1 ± 97.46 ; $n = 14$ neurons; L1342P + M, 628.9 ± 58.85 ; $n = 24$ neurons; two-way ANOVA with Tukey's multiple comparisons; ** $p = 0.0040$; Fig. 4F).

Notably, we did not observe major changes in the maximum number of AP firings triggered in the WT neurons cocultured with microglia compared with WT neuron alone (WT, 8.25 ± 0.92 APs; $n = 12$ neurons; two differentiations; WT + M, 9.50 ± 0.52 APs; $n = 18$ neurons; two differentiations; two-way ANOVA with Tukey's multiple comparisons; n.s., $p = 0.7172$; Fig. 4G). But interestingly, we observed a decrease in the maximum number of AP firings triggered by increasing current injections in the L1342P neuron cocultured with microglia, showing a 21% decrease over Nav1.2-L1342P neurons alone (L1342P, 13.86 ± 1.04 ; $n = 14$ neurons; L1342P + M, 10.68 ± 0.81 ; $n = 25$ neurons; two-way ANOVA with Tukey's multiple comparisons; * $p = 0.0421$; Fig. 4G). For a direct comparison between the WT and Nav1.2-L1342P neurons, we observed an increasing number of triggered maximum AP firings in Nav1.2-L1342P neurons (Fig. 4G), which recapitulate our published results (Que et al., 2021). Together, our data suggest that hiPSC-derived human microglia selectively reduce repetitive firings in hiPSC-derived neurons carrying the seizure-related Nav1.2-L1342P mutation.

It is possible that the addition of microglia may affect the intrinsic electrical properties of the neurons, such as AP amplitude, threshold, speed, rise time, or afterhyperpolarization (AHP), which could lead to the reduction in AP firing. To investigate this, we performed an analysis of single AP waveforms from WT and L1342P neurons, both with and without microglia. However, we did not observe statistically significant differences in single AP parameters resulting from the presence of microglia, indicating that microglia do not affect single neuronal AP waveform parameters in our model.

Given the major changes observed in the repetitive firing patterns of L1342P mutant neurons, we analyzed key intrinsic properties in the waveforms from multiple APs. Our analysis revealed significant changes consistent with reduced repetitive neuronal firing and sodium current density. We detected a trend toward depolarization of the AP voltage threshold, specifically in the first, second, and final APs. However this effect was small (~ 4.5 mV or $\sim 15\%$) and did not reach significance (first AP: L1342P, -37.22 ± 1.59 ; $n = 14$ neurons; L1342P + M, -33.87 ± 1.54 ; $n = 19$ neurons; $p = 0.1525$; second AP: L1342P, -30.44 ± 1.83 ; $n = 14$ neurons; L1342P + M, -26.54 ± 1.59 ; $n = 19$ neurons; $p = 0.1219$; final AP: L1342P, -24.63 ± 2.07 ; $n = 14$ neurons; L1342P + M, -20.99 ± 1.94 ; $n = 19$ neurons, $p = 0.219198$; multiple unpaired Student's t tests with Holm–Šidák correction for multiple comparisons; Fig. 4H). Even though they were not statistically significant, a minor depolarized shift in voltage threshold might suggest a reduced capability to fire in the L1342P + M group. We then analyzed the AHP of the repetitive AP trains, and we determined that the AHP following the final AP was

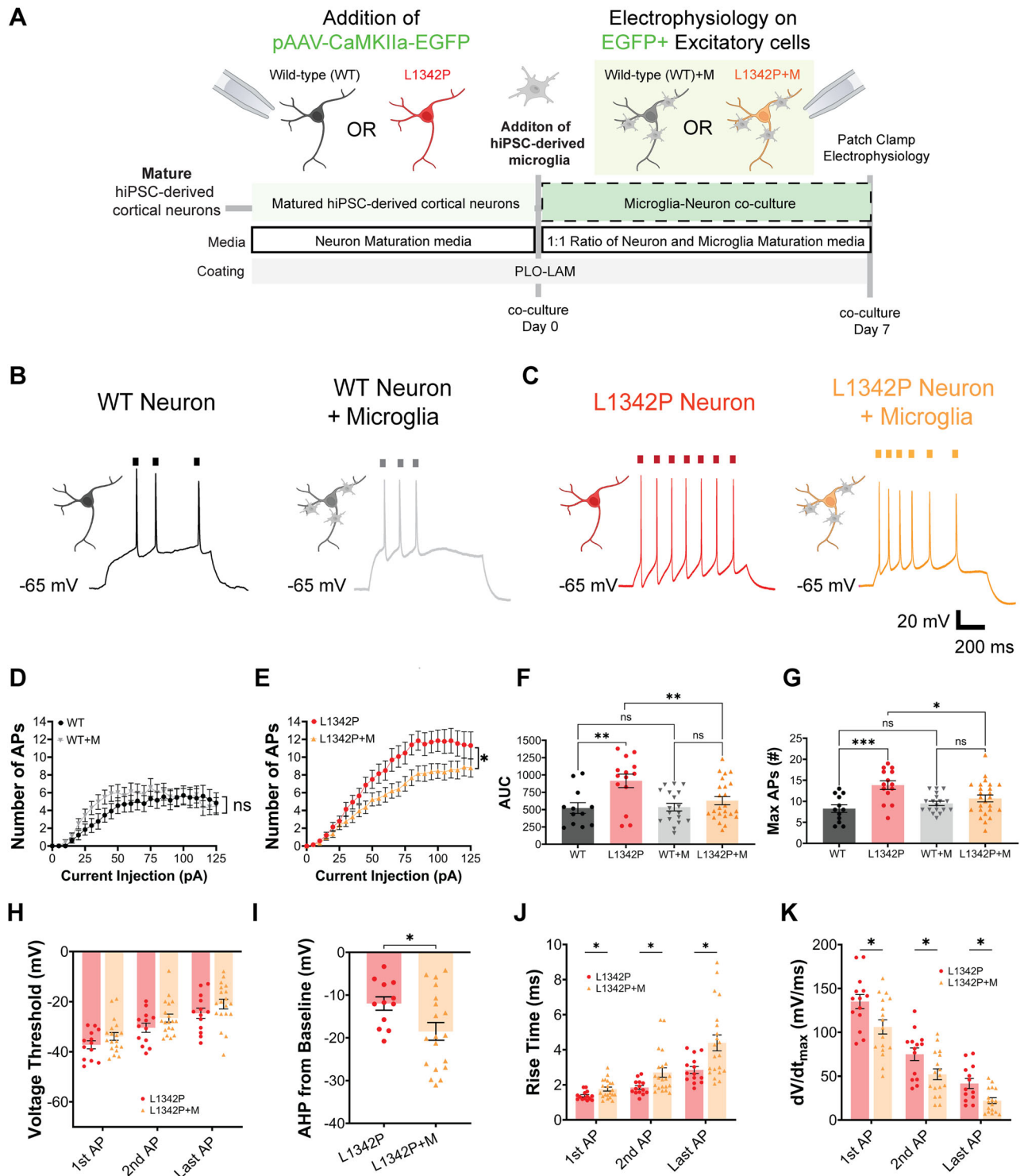


Figure 4. The repetitive firing of hiPSC-derived Nav1.2-L1342P neurons is reduced when cocultured with microglia. **A**, hiPSC-derived cortical neurons were transduced with an AAV-CaMKIIa-EGFP to allow the detection of excitatory neuronal populations for patch-clamp electrophysiology. Neurons and microglia were cocultured for 7 d before patch-clamp measurements. **B**, Representative AP firings from hiPSC-derived control (WT) cortical neurons alone (left) and with microglia (right). **C**, Representative AP firings from hiPSC-derived Nav1.2-L1342P cortical neurons alone (left) and with microglia (right). **D**, In WT neurons, current injection-triggered AP firing remains relatively unchanged regardless of microglia coculture (WT, $n = 12$ neurons; two differentiations; WT + M, $n = 18$ neurons; two differentiations). **E**, In Nav1.2-L1342P neurons, current injection-triggered AP firing is reduced when cocultured with microglia (L1342P, $n = 14$ neurons; two differentiations; L1342P + M, $n = 25$ neurons; two differentiations). **F**, AUC summary of the number of APs versus current injection for all conditions. Each dot corresponds to one neuron. **G**, Maximum AP number per cell across increasing current injections until 125 pA. **H**, Voltage thresholds for first, second, and last APs exhibited a consistent trend toward depolarization in the L1342P + M group. **I**, AHP from the baseline was decreased in the L1342P + M conditions. **J**, The rise time was increased in each successive AP in the L1342P + M conditions, indicating a longer time for the AP to take place. **K**, The dV/dt_{max} (mV/ms) as a function of AP# measured at 85 pA current injection decreased with each AP firing in the L1342P + M conditions. Each dot represents an individual AP firing. Data are presented as mean \pm SEM. Data in panels **D** and **E** were analyzed by repeated-measures of two-way ANOVA, with data pooled from at least two differentiations per condition. Data in **F** and **G** were analyzed using two-way ANOVA with Tukey's multiple comparisons. Data in panels **H**, **J**, and **K** were analyzed using multiple t tests with Holm-Šidák correction for multiple comparisons, while data in **I** was analyzed with an unpaired Student's t test. * $p < 0.05$; ** $p < 0.01$; *** $p < 0.001$; and n.s. (not significant).

significantly more hyperpolarized in the presence of microglia (L1342P, -11.97 ± 1.561 ; $n = 12$ neurons; L1342P + M, -19.69 ± 2.079 ; $n = 19$ neurons; unpaired Student's *t* test; $*p = 0.0324$; Fig. 4I). A more hyperpolarized AHP indicates that neurons with microglia take more time to repolarize back to the baseline after simulation, suggesting a reduced excitability phenotype.

Additionally, we analyzed the kinetics of AP rising phase, since it is primarily driven by the influx of sodium ions. We observed a decrease in the speed of the rising phase of the first, second, and final APs in the repetitive firing trace, as indicated by the increased rise time and decreased maximum dV/dt in the group of L1342P + M (rise time first AP: L1342P, 1.376 ± 0.068 ms; $n = 14$ neurons; L1342P + M, 1.759 ± 0.113 ms; $n = 21$ neurons; $*p$ adjusted = 0.0135; second AP: L1342P, 1.852 ± 0.109 ; $n = 14$ neurons; L1342P + M, 2.704 ± 0.268 ms; $n = 21$ neurons; unpaired Student's *t* test; $*p$ adjusted = 0.0134; and final AP: L1342P, 2.846 ± 0.199 ms; $n = 14$ neurons; L1342P + M, 4.393 ± 0.455 ; $n = 21$ neurons; $*p = 0.0129$; multiple unpaired Student's *t* test with Holm-Šidák correction for multiple comparisons; Fig. 4J). Correspondingly, the maximum dV/dt was also decreased in the first, second, and final AP waveforms (Max dV/dt first AP: L1342P, 135.00 ± 8.07 mV/ms; $n = 14$ neurons; L1342P + M, 106.12 ± 7.16 mV/ms; $n = 17$ neurons; $*p = 0.0353$; second AP: 74.98 ± 7.16 mV/ms; $n = 14$ neurons; L1342P + M, 52.18 ± 6.15 ; $n = 17$ neurons; $*p = 0.0354$; and final AP: 39.32 ± 5.79 ; $n = 14$ neurons; L1342P + M, 22.08 ± 3.33 ; $n = 17$ neurons; $*p = 0.0345$; multiple unpaired Student's *t* tests with Holm-Šidák correction for multiple comparisons; Fig. 4K). These data indicate an alteration of sodium channel including reduced current density and less availability of sodium channel, further

suggesting a reduced neuronal excitability phenotype in neurons with microglia.

These findings demonstrate that the addition of microglia significantly modulates repetitive firing, by reducing the speed of AP firing. Our data align with our observations of decreased sodium currents (shown in the next section), indicating that the presence of microglia has a significant effect on lowering repetitive AP firings, likely through their effects on sodium channels. Taken together, these alterations in the AP waveform characteristics suggest reduced intrinsic neuronal excitability of the SCN2A-L1342P neurons cocultured with microglia, aligning with our observation that fewer AP firings were triggered over time in response to the same current inputs.

The presence of hiPSC-derived microglia reduces the maximum sodium current density in hiPSC-derived neurons carrying the Nav1.2-L1342P mutation

It is known that sodium channel density may affect the firing properties of neurons (Motipally et al., 2019). Moreover, studies have suggested that adding microglia to neurons may alter gene expression patterns (Baxter et al., 2021). Thus, the presence of microglia may lead to alternations of genes/protein levels involved in neuronal electrical activity, such as those that encode ion channels. Therefore, we performed experiments to study the sodium channel activation and maximum sodium current density in neurons alone and in coculture with microglia (Fig. 5A). We obtained the sodium channel activation traces over varying voltage for L1342P neurons in isolation (Fig. 5B) and in coculture with microglia (Fig. 5C). This allowed us to measure the maximum voltage-gated sodium channel current density in

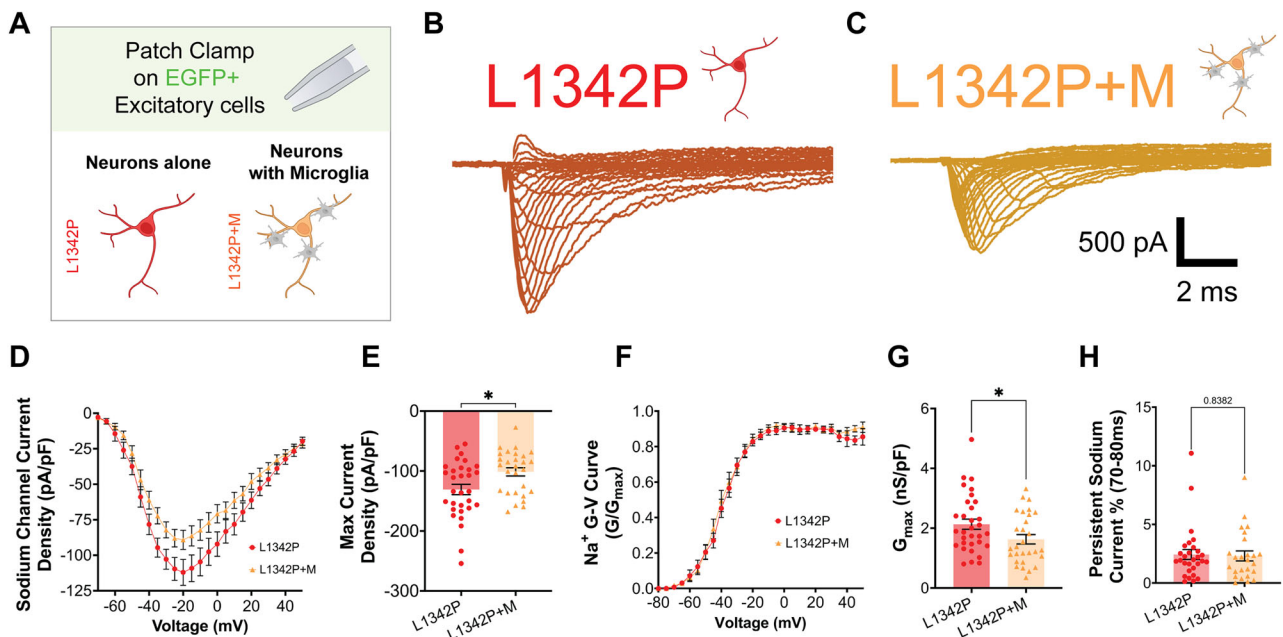


Figure 5. hiPSC-derived Nav1.2-L1342P neurons display reduced sodium current density with microglia coculture. **A**, The patch clamp was performed on hiPSC-derived cortical neurons transduced with CaMKII virus to selectively label excitatory neuron populations. **B**, Representative sodium current trace from Nav1.2-L1342P cortical neurons. **C**, Representative sodium current trace from Nav1.2-L1342P cortical neurons cocultured with hiPSC-derived microglia. In both panels **B** and **C**, the outward current was blocked using tetraethylammonium chloride in the bath solution. **D**, Average peak sodium current density versus voltage ($I-V$) curves for Nav1.2-L1342P neurons with or without microglia coculture. **E**, The maximum current density was significantly reduced in Nav1.2-L1342P neurons in coculture with microglia (right) (L1342P: $n = 31$ neurons, three differentiations; L1342P + M, $n = 28$ neurons from two differentiations). **F**, Normalized G/G_{max} versus voltage curves, showing no notable difference between L1342P and L1342P + M (with microglia) conditions. **G**, The maximum conductance (G_{max}), normalized to cell capacitance, was significantly decreased in L1342P neurons cocultured with microglia. **H**, The persistent current, measured as a percentage of the peak amplitude at 70–80 ms after the peak sodium transient current, showed no change between the L1342P and L1342P + M conditions. Data are presented as mean \pm SEM. Data in **E**, **G**, and **H** was analyzed by unpaired Student's *t* test, with each dot representing an individual neuron. Data were collected from at least two independent differentiations per genotype. $*p < 0.05$.

Nav1.2-L1342P hiPSC-derived neurons with or without microglia (Fig. 5D). Interestingly, we observed a decrease in the maximum sodium current density in Nav1.2-L1342P neurons cocultured with microglia (L1342P, -130.8 ± 8.578 pF/pA; $n = 31$ neurons; L1342P + M, -101.4 ± 6.869 pF/pA; $n = 28$ neurons; $*p = 0.0107$; unpaired Student's *t* test; Fig. 5E). On the other hand, we found that the presence of microglia only slightly reduced the current density of WT neurons, which did not reach a statistically significant difference (WT, -118.2 ± 12.03 pA/pF $n = 30$ neurons; WT + M, -95.35 ± 10.48 pA/pF; $n = 19$ neurons; unpaired Student's *t* test; n.s., $p = 0.1933$). This reduced maximum sodium channel current density in Nav1.2-L1342P neuron coculture with microglia may serve as a possible mechanism underlying decreased intrinsic excitability of neurons carrying the Nav1.2-L1342P mutation when cocultured with microglia.

To further test whether microglia could alter the voltage dependence of channel activation, the normalized G - V curve (G/G_{\max} vs voltage) was plotted. No notable difference was observed between the L1342P and L1342P + M on the channel activation curve (Fig. 5F). Additionally, to further confirm the decrease in max sodium current density, we calculated G_{\max} (normalized for cell capacitance). We observed the same trend that microglia significantly reduce G_{\max} (L1342P, 2.132 ± 0.172 nS/pF; $n = 31$ neurons; L1342P + M, 1.627 ± 0.156 ; $n = 28$ neurons; $*p = 0.0305$; unpaired Student's *t* test; Fig. 5G). Since the maximum sodium current measurement could suffer from the potential space clamping issue, we subsequently assessed the persistent sodium current. Our results revealed no significant change in the persistent sodium currents percentage between the L1342P neurons and L1342P + M conditions (L1342P, $2.429 \pm 0.4244\%$; $n = 29$ neurons; L1342P + M, $2.305 \pm 0.4215\%$; $n = 25$ neurons; n.s., $p = 0.8382$; unpaired Student's *t* test; Fig. 5H). Taken together, our results indicate that microglia do not seem to change the biophysical properties of the sodium channels in

neurons but rather reduce the magnitude of max sodium current density and max conductance.

Sodium channel expression is reduced within the AIS of hiPSC-derived L1342P neurons cocultured with microglia

The AIS is a specialized region within the neuronal axon where key sodium channels are expressed, and APs are initiated (Harley et al., 2023). Changes in the components (e.g., sodium channel) of AIS are likely to impact neuronal excitability. Because we observed changes in the repetitive action firing when the cortical neurons were cocultured with microglia, it is possible that the presence of microglia may alter the distribution and expression of AIS components of the neuron needed for AP firing. To further probe a possible mechanism to explain of reduced repetitive firings in L1342P neurons, we investigated the expression of sodium channels with an antibody targeting Pan Nav, allowing the identification of all vertebrate sodium channels. This assessment was done relative to the localization of the AIS, which can be identified with the scaffolding protein ANK-G.

Immunocytochemistry was performed on hiPSC-derived cortical neurons matured for 45+ d. Neurons were labeled using somatodendritic marker MAP2 (Fig. 6A). Using confocal microscopy, we obtained images that allowed us to determine the AIS length and the localized expression of sodium channels in L1342P neurons alone (Fig. 6A, top) or in coculture with microglia (Fig. 6A, bottom). We observed that the AIS length remained relatively unchanged between the L1342P neurons alone and in coculture with microglia (L1342P, 31.72 ± 1.43 μm ; $n = 42$ neurons; L1342P + M, 35.97 ± 1.83 μm ; $n = 21$ neurons; unpaired Student's *t* test; n.s., $p = 0.0822$; Fig. 6B). Interestingly, the Pan Nav intensity was significantly reduced within the AIS region (L1342P, 0.1777 ± 0.01783 ; $n = 42$ neurons; L1342P + M, 0.1009 ± 0.01793 ; $n = 19$ neurons; unpaired Student's *t* test; $*p = 0.0344$; Fig. 6C), likely indicating that

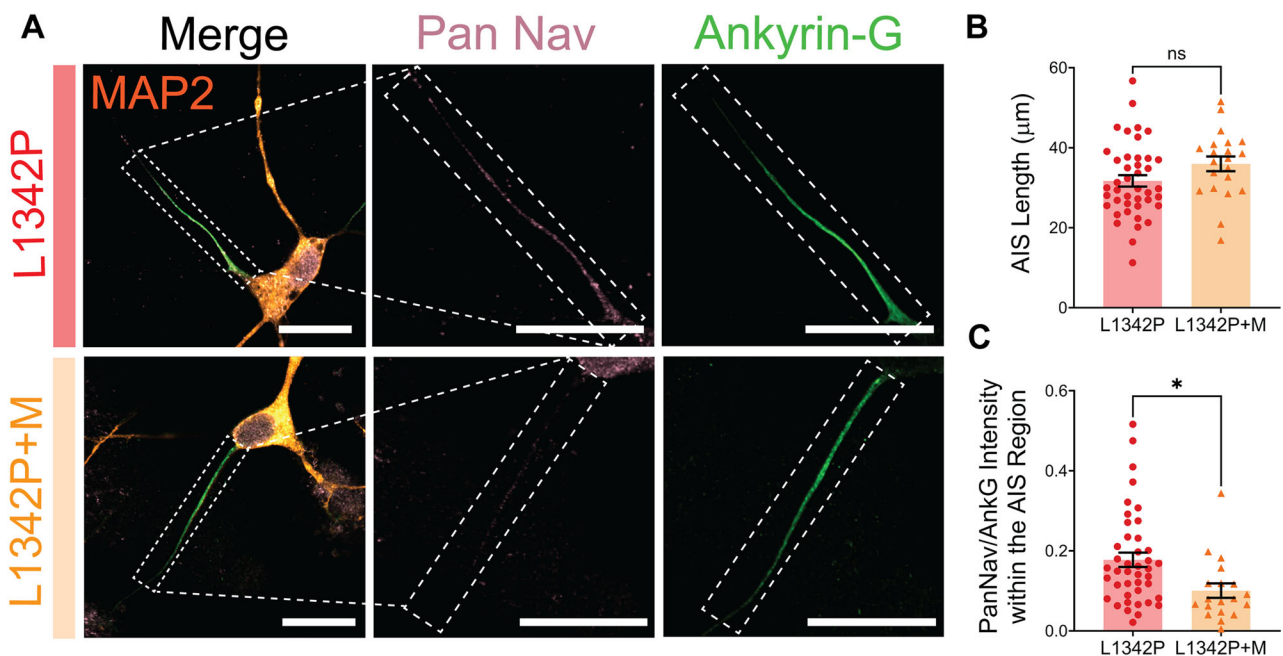


Figure 6. The intensity of the PanNav/AnkG in the AIS is reduced in the hiPSC-derived Nav1.2-L1342P neurons cocultured with microglia. **A**, Representative images of L1342P alone (top) and L1342P neurons cocultured with microglia (bottom) were shown. MAP2 (orange), Pan Nav (magenta), and ANK-G (green). Scale bar, 20 μm . **B**, No notable change was observed for AIS length in L1342P neurons with or without microglia coculture. **C**, The normalized PanNav/AnkG intensity in the AIS region was reduced in the hiPSC-derived L1342P neurons in microglia coculture conditions. Each dot corresponds to one neuron. Data are presented as mean \pm SEM. Data in **B–C** were analyzed by unpaired Student's *t* test. $*p < 0.05$ and n.s. (not significant)

microglia may exert an effect on sodium channel distribution or expression along this unit.

L1342P neuronal cultures exhibit increased extracellular glutamate release

During periods of intense neuronal hyperactivity, such as seizures, neurons could release excess glutamate (Barker-Haliski and White, 2015). Microglia express a diverse set of glutamate receptors, including ionotropic (Ca^{2+}) glutamate receptors like AMPA, kainate, or N-methyl-D-aspartate (NMDA) and metabotropic glutamate receptors (Pocock and Kettenmann, 2007; Czapski and Strosznajder, 2021). Studies suggest that glutamate facilitates microglial process extension in the CA1 region of the

hippocampus (Eyo et al., 2014). It is thus possible that these microglial receptors could be stimulated by glutamate to trigger changes in microglial morphology (Beppu et al., 2013; X. Zhang et al., 2020) as well altering calcium signals (Logiacco et al., 2021). However, it is not known whether hiPSC-derived neurons carrying epilepsy-associated *SCN2A* mutation would release excessive glutamate.

We thus carried out an experiment to measure the glutamate release of WT and Nav1.2-L1342P neurons (Fig. 7A). Controlling for basal glutamate in the media, we observed that the mutant Nav1.2-L1342P neurons released more glutamate after 48 h than controls, almost 1.5-fold increase (WT, 1.000 ± 0.032 ; $n = 18$ wells; two differentiations; L1342P, 1.584 ± 0.068 ; $n = 18$

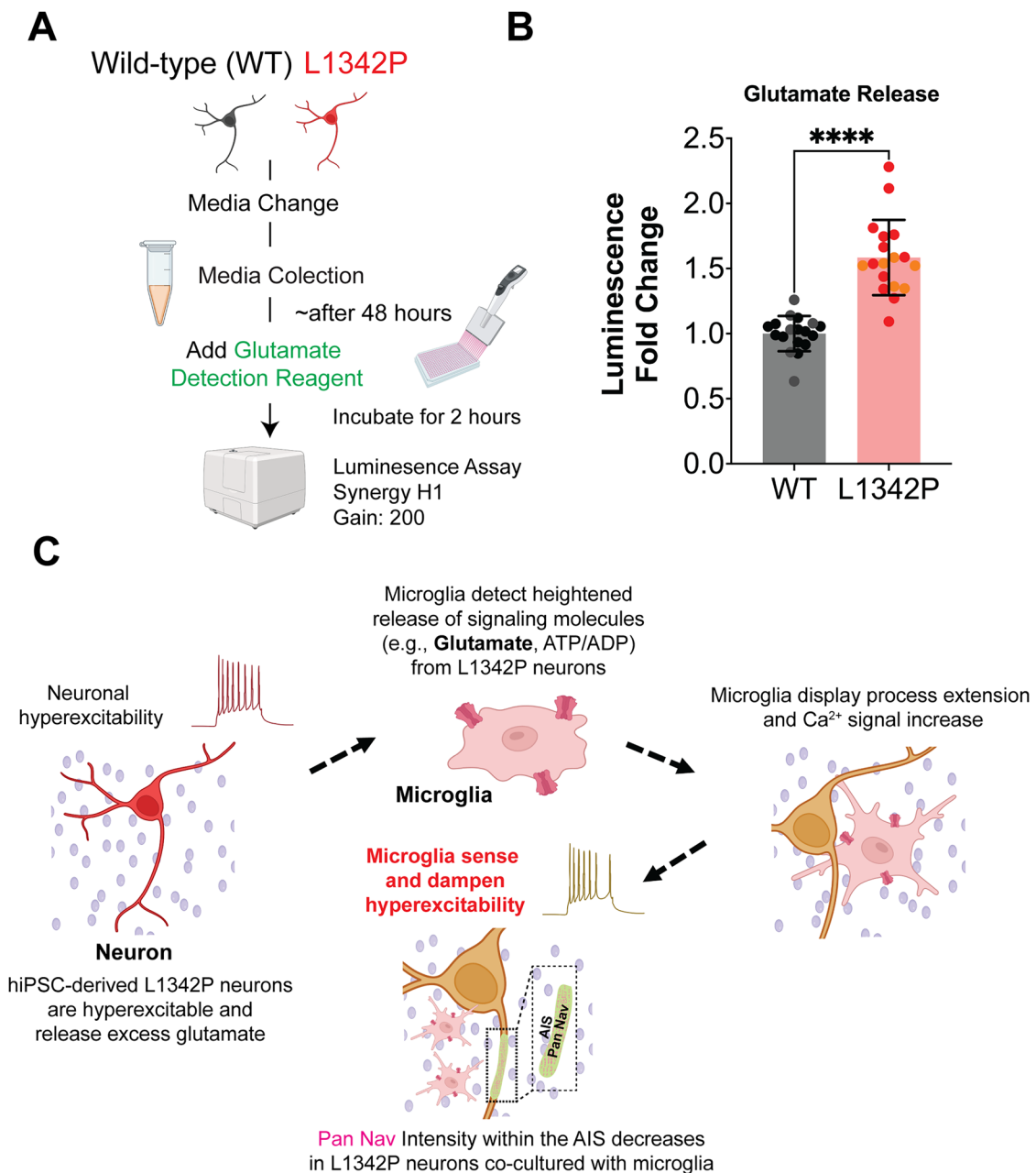


Figure 7. hiPSC-derived Nav1.2-L1342P neuron cultures produce excessive extracellular glutamate. **A**, Experimental design schematic. **B**, Glutamate release from hiPSC-derived WT or L1342P neurons over 48 h, presented as fold change in luminescence (WT, $n = 18$ wells, from two differentiations; L1342P, $n = 18$ wells, from two differentiations). Data are presented as mean \pm SEM. Statistical analysis conducted using unpaired Student's *t* test. **C**, Proposed possible mechanism illustrating microglial sensing and dampening hyperexcitability of neurons carrying epilepsy-associated *SCN2A* mutation.

wells; two differentiations (each dot represents one well); unpaired Student's *t* test; *****p* < 0.0001; Fig. 7B). Our findings thus reveal that the hyperexcitable neurons carrying an SCN2A-L1342P mutation release more glutamate than control neurons, which may trigger glutamate-related signal pathways to mediate microglial responses (Fig. 7C).

Discussion

In this current study, we developed a coculture model combining WT hiPSC-derived microglia and cortical neurons with a hyperexcitable phenotype due to the SCN2A-L1342P mutation. To our knowledge, this is the first *in vitro* study to investigate how human microglia respond and influence hyperexcitable neurons carrying a disease-causing mutation identified in patients with genetic epilepsy. Our findings have demonstrated that microglia can sense and respond to hyperexcitable neurons by increasing branch length, likely through mechanisms involving glutamate and calcium signaling. Additionally, we observed that microglia significantly dampened the repetitive AP firings of neurons carrying the epilepsy-associated Nav1.2-L1342P mutation while having minimal impact on WT neurons. We further show that hiPSC-derived cortical neurons carrying the epilepsy-associated Nav1.2-L1342P mutation have reduced sodium current density when cocultured with human microglia. This occurs along with a reduction of sodium channel expression within the AIS region of neurons. Together, our results underscore the significance of neuron microglia interactions in understanding disease manifestation and suggest a potential mechanism by which microglia alleviate neuronal hyperexcitability.

Previous studies have shown that microglia can experience morphological changes in response to neuronal activity (Nebling et al., 2023). In a kainic acid (KA)-triggered seizure model, changes in microglia morphology manifested as an extended length and increased number of microglial branch processes (Eyo et al., 2014). Our findings align with observations in these mouse models, showing microglial processes extension when cocultured with neurons carrying epilepsy-associated Nav1.2 mutation. By recapitulating key morphological findings from seizure-related mouse models in our human cell-based *in vitro* model, we contribute to a deeper understanding of the pathophysiological mechanisms underlying microglial responses in seizure disorders.

Microglial calcium signaling can undergo dynamic changes in response to their environment, including in response to the excitability of the neurons in live mice (Umpierre et al., 2020). In response to electrical stimulation, a population of microglia endogenously expressing the Ca²⁺ indicator GCaMP6 exhibited noticeable Ca²⁺ elevations in neonatal mice (Logiacco et al., 2021). Furthermore, microglia have been observed to experience calcium fluctuations in response to changes in neuronal activity induced through pharmacological and chemogenetic methods. For example, increased neuronal activity (either in KA-induced status epilepticus or genetic manipulations using Gq-DREADD activation) could trigger the elevation of calcium signal amplitude and AUC in microglia (Umpierre et al., 2020). Interestingly, reduced neuronal activity through isoflurane anesthesia or Gi-DREADD inhibition has also been shown to increase microglial calcium activity (Umpierre et al., 2020). These observations highlight the dynamic nature of microglial responses to bimodal alterations in neuronal excitability. Notably, these calcium responses were mainly localized to microglial processes rather than the soma (Umpierre et al., 2020) and probably mediated by UDP-P2Y6 signaling (Umpierre et al., 2023). To further

provide insights into microglial responses to neuronal activity in a more pathophysiological context, we use an intrinsically hyperexcitable human neuronal model that does not require external stimuli. Despite the considerable species differences between human and rodent microglia, our study revealed a consistent finding that calcium signal was increased in the presence of hyperexcitable neurons and mainly localized in the microglial processes.

While the exact mechanisms and pathways underlying microglial responses to hyperexcitable neurons are not yet fully understood, our study provided interesting results allowing us to propose a possible mechanism. We suggest that excess extracellular glutamate (as well as potentially ATP/ADP), released by the hyperexcitable neurons carrying the SCN2A mutation, may initiate signaling cascade in microglia, prompting morphological changes and alter calcium dynamics. The presence of microglia appears to reduce sodium current density and decrease the expression of sodium channels in the AIS region, possibly leading to the reduction of repetitive AP firings (Fig. 7C). The specific mechanisms by which microglia induce changes in neuronal activity and gene expression remain to be elucidated, presenting an interesting direction for future research.

While our study found that human microglia can mitigate the excitability of hyperexcitable neurons carrying the epilepsy-associated Nav1.2-L1342P mutation, the influences of microglia on neuronal excitability and seizure phenotypes are quite complex and context-dependent. In our human cell-based model, we observed that the presence of microglia could reduce the excitability of the hyperexcitable Nav1.2-L1342P neurons, suggesting a presumably beneficial role of microglia in dampening neuronal hyperexcitability. This aligns with existing literature suggesting a favorable impact of microglia on seizure modulation. For instance, pharmacological (CSF1R inhibitor, PLX3397) and genetic approaches to deplete microglia from mice lead to an increase in neuronal activity and seizures (Liu et al., 2020; W. Wu et al., 2020; Gibbs-Shelton et al., 2023), while their repopulation conferred seizure protection (W. Wu et al., 2020; Gibbs-Shelton et al., 2023). Additionally, microglial process extensions seem to be neuroprotective, as their absence seen in P2RY12 knock-out mice worsened KA-induced seizure outcomes (Eyo et al., 2014).

Interestingly, contradictory to the beneficial role of microglia, it has been suggested that microglia can also play a detrimental role in epileptogenesis (Vezzani et al., 2013). Several studies implicate that the release of proinflammatory cytokines by microglia could be potential seizure-triggering factors (De Simoni et al., 2000; Libbey et al., 2011). For example, in a mouse model of acquired temporal lobe epilepsy triggered by KA administration, microglia were found to exert proconvulsive effects through the release of proinflammatory mediator cytokines, contributing to severe status epilepticus (Henning et al., 2023). Similar increases in proinflammatory mediator cytokines could also be observed in surgical tissue resected from cases of human temporal lobe epilepsy, further highlighting the role of inflammation in seizure formation (Kan et al., 2012). These studies together suggest a possible detrimental role of microglia as a seizure trigger. Further studies with diverse models are necessary to elucidate the precise role of microglia in different types of seizures and to consolidate the discrepancy among distinct studies.

While our results reveal interesting interactions between microglia and neuron, they have limitations and open additional questions. Our model is an acute exposure of microglia to neurons, thus interpreting chronic effects of interactions between

microglia and hyperexcitable neurons should be taken with caution. As an *in vitro* study, it is also worth noting that microglial morphology in our model cannot be directly compared with microglial morphology *in vivo* (Wyatt-Johnson et al., 2017). Moreover, this study did not comprehensively examine the whole array of microglia and neuron functions. For example, since we identified a presumably beneficial role of microglia in our disease model, we did not assess the microglial cytokine release in our study, given that cytokine release has been shown to exacerbate neuronal hyperexcitability.

Space clamp artifacts occur when sodium channels are not fully clamped, causing current from distal compartments to impact the voltage sweep. Space clamp artifacts are a well-documented challenge when recording currents from neurons, which often have complex morphology. This phenomenon has been observed in several hiPSC-derived neuron studies with similar experimental designs that compare the effects of Nav channel variants on sodium channel current densities to their WT channel counterparts (H. W. Zhao et al., 2015; Y. Sun et al., 2016; Meents et al., 2019; Xie et al., 2020; Asadollahi et al., 2023). Although we also found space clamp effect in our study, it exists in both our control and experimental conditions. Thus, our comparisons between the groups are still informative. To reduce space clamp artifacts, researchers have isolated somatic currents from the AIS, though at the expense of removing distal contributions to the total sodium current density values (Milescu et al., 2010; Meents et al., 2019). Others have also attempted to record from smaller and less mature neurons with simpler morphology to reduce the proportion of distal sodium channels, resulting in reduced but still noticeable space clamp issues (H. W. Zhao et al., 2015). Alternatively, studies have instead focused on measuring persistent sodium currents, which are less susceptible to space clamping effects. These are typically driven by SCN8A in mature neurons (Tidball et al., 2020) or by aberrant Nav channels with slow inactivation (Qu et al., 2024), neither of which apply to the SCN2A-L1342P genetic variant used in our study.

Furthermore, our study intentionally did not utilize microglia derived from hiPSCs carrying the Nav1.2-L1342P mutation, as clear evidence suggests that Nav1.2 expression was minimal in microglia (Black et al., 2009; Black and Waxman, 2012, 2013; Abud et al., 2017; Grubman et al., 2020; Dräger et al., 2022). However, while highly unlikely, we cannot rule out that human microglia carrying the Nav1.2-L1342P might unexpectedly act differently than control (WT) microglia. While the exact mechanism is unknown, other studies have shown that coculturing microglia with neurons in an assembloid model could influence synapse remodeling-related gene expression (Sabate-Soler et al., 2022). Additionally, we did not explore other potential mechanisms which could explain the reduction of electrical activity. For instance, it is possible that microglia could modulate neuronal activity through the removal of excessive synapses (J. Wu et al., 2024), as evidenced by studies in a hyperexcitable SCN2A-deficient mouse model (Eaton et al., 2021; J. Zhang et al., 2021; Ma et al., 2022). Furthermore, we did not investigate alterations in microglial Gi signaling, which have been recently linked to dampening of neuronal activity and impairing of neuronal synchronization (Merlini et al., 2021; S. Zhao et al., 2024). Future studies are needed to further dissect the mechanism underlying microglial-mediated changes in neurons.

As the influence of microglia on neuronal excitability is complex, our findings may or may not be generalized to other types of epilepsies (e.g., other genetic epilepsies caused by Nav1.1/Nav1.6 mutations or distinct acquired epilepsy), because microglia's

effects may vary depending on the context. However, evidence exists to support a hypothesis that a common effect of microglial regulation of hyperexcitable neurons may exist. It was reported that in an *in vitro* cell culture model related to seizures, the addition of primary microglia can decrease the mean firing rate of WT cortical neurons exposed to glutamate (a distinct hyperexcitable neuron model; Badimon et al., 2020), suggesting a possible generalization of our findings.

In summary, our study unveils, for the first time, the specific beneficial effect of microglia in reducing the excitability of hyperexcitable hiPSC-derived cortical neurons carrying the epilepsy-related Nav1.2-L1342P mutation. These findings underscore the significance of neuron–microglia interaction and emphasize the necessity of integrating hiPSC-derived microglia into neuron-based disease models. Such a platform not only provides a more comprehensive and pathophysiologically relevant system but also offers a promising avenue for testing therapeutic interventions utilizing hiPSC-derived neurons and microglia coculture.

References

- Abud EM, et al. (2017) iPSC-derived human microglia-like cells to study neurological diseases. *Neuron* 94:278–293.e9.
- Asadollahi R, et al. (2023) Pathogenic SCN2A variants cause early-stage dysfunction in patient-derived neurons. *Hum Mol Genet* 32:2192–2204.
- Badimon A, et al. (2020) Negative feedback control of neuronal activity by microglia. *Nature* 586:417–423.
- Barker-Haliski M, White HS (2015) Glutamatergic mechanisms associated with seizures and epilepsy. *Cold Spring Harb Perspect Med* 5:a022863.
- Baxter PS, Dando O, Emelianova K, He X, McKay S, Hardingham GE, Qiu J (2021) Microglial identity and inflammatory responses are controlled by the combined effects of neurons and astrocytes. *Cell Rep* 34:108882.
- Beppu K, et al. (2013) Expression, subunit composition, and function of AMPA-type glutamate receptors are changed in activated microglia; possible contribution of GluA2 (GluR-B)-deficiency under pathological conditions. *Glia* 61:881–891.
- Black JA, Liu S, Waxman SG (2009) Sodium channel activity modulates multiple functions in microglia. *Glia* 57:1072–1081.
- Black JA, Waxman SG (2012) Sodium channels and microglial function. *Exp Neurol* 234:302–315.
- Black JA, Waxman SG (2013) Noncanonical roles of voltage-gated sodium channels. *Neuron* 80:280–291.
- Chai X, Xiao Z, Zhao Q, Wang J, Ding D, Zhang J (2023) Cognitive impairment as a comorbidity of epilepsy in older adults: analysis of global and domain-specific cognition. *Epileptic Disord* 25:65–73.
- Chen T-W, et al. (2013) Ultrasensitive fluorescent proteins for imaging neuronal activity. *Nature* 499:295–300.
- Chen R, Peng B, Zhu P, Wang Y (2023) Modulation of neuronal excitability by non-neuronal cells in physiological and pathophysiological conditions. *Front Cell Neurosci* 17:1133445.
- Christensen J, et al. (2023) Estimates of epilepsy prevalence, psychiatric co-morbidity and cost. *Seizure* 107:162–171.
- Crawford K, et al. (2021) Computational analysis of 10,860 phenotypic annotations in individuals with SCN2A-related disorders. *Genet Med* 23:1263–1272.
- Czapski GA, Strosznajder JB (2021) Glutamate and GABA in microglia-neuron cross-talk in Alzheimer's disease. *Int J Mol Sci* 22:11677.
- De Simoni MG, Perego C, Ravizza T, Moneta D, Conti M, Marchesi F, De Luigi A, Garattini S, Vezzani A (2000) Inflammatory cytokines and related genes are induced in the rat hippocampus by limbic status epilepticus. *Eur J Neurosci* 12:2623–2633.
- Dräger NM, et al. (2022) A CRISPRi/a platform in human iPSC-derived microglia uncovers regulators of disease states. *Nat Neurosci* 25:1149–1162.
- Eaton M, et al. (2021) Generation and basic characterization of a gene-trap knockout mouse model of Scn2a with a substantial reduction of voltage-gated sodium channel Nav1.2 expression. *Genes Brain Behav* 20:e12725.
- Epifanio R, Giorda R, Merlano MC, Zanotta N, Romaniello R, Marelli S, Russo S, Cogliati F, Bassi MT, Zucca C (2021) SCN2A pathogenic variants and epilepsy: heterogeneous clinical, genetic and diagnostic features. *Brain Sci* 12:18.

- Eyo UB, Peng J, Swiatkowski P, Mukherjee A, Bispo A, Wu L-J (2014) Neuronal hyperactivity recruits microglial processes via neuronal NMDA receptors and microglial P2Y12 receptors after status epilepticus. *J Neurosci* 34:10528–10540.
- Gibbs-Shelton S, et al. (2023) Microglia play beneficial roles in multiple experimental seizure models. *Glia* 71:1699–1714.
- Grubman A, et al. (2020) A CX3CR1 reporter hESC line facilitates integrative analysis of in-vitro-derived microglia and improved microglia identity upon neuron-glia co-culture. *Stem Cell Reports* 14:1018–1032.
- Haenseler W, et al. (2017) A highly efficient human pluripotent stem cell microglia model displays a neuronal-co-culture-specific expression profile and inflammatory response. *Stem Cell Reports* 8:1727–1742.
- Harley P, Kerins C, Gatt A, Neves G, Riccio F, Machado CB, Cheesbrough A, R'Bibo L, Burrone J, Lieberam I (2023) Aberrant axon initial segment plasticity and intrinsic excitability of ALS hiPSC motor neurons. *Cell Rep* 42:113509.
- Hendrickx DA, Schuurman KG, van Draanen M, Hamann J, Huitinga I (2014) Enhanced uptake of multiple sclerosis-derived myelin by THP-1 macrophages and primary human microglia. *J Neuroinflammation* 11:64.
- Henning L, et al. (2023) Reactive microglia are the major source of tumor necrosis factor alpha and contribute to astrocyte dysfunction and acute seizures in experimental temporal lobe epilepsy. *Glia* 71:168–186.
- Jairaman A, et al. (2022) TREM2 regulates purinergic receptor-mediated calcium signaling and motility in human iPSC-derived microglia. *Elife* 11:e73021.
- Kan AA, et al. (2012) Protein expression profiling of inflammatory mediators in human temporal lobe epilepsy reveals co-activation of multiple chemokines and cytokines. *J Neuroinflammation* 9:207.
- Knowles JK, et al. (2022) Precision medicine for genetic epilepsy on the horizon: recent advances, present challenges, and suggestions for continued progress. *Epilepsia* 63:2461–2475.
- Libbey JE, Kennett NJ, Wilcox KS, White HS, Fujinami RS (2011) Interleukin-6, produced by resident cells of the central nervous system and infiltrating cells, contributes to the development of seizures following viral infection. *J Virol* 85:6913–6922.
- Liu M, Jiang L, Wen M, Ke Y, Tong X, Huang W, Chen R (2020) Microglia depletion exacerbates acute seizures and hippocampal neuronal degeneration in mouse models of epilepsy. *Am J Physiol Cell Physiol* 319:C605–C610.
- Logiaco F, Xia P, Georgiev SV, Franconi C, Chang Y-J, Ugursu B, Sporbert A, Kühn R, Kettenmann H (2021) Microglia sense neuronal activity via GABA in the early postnatal hippocampus. *Cell Rep* 37:110128.
- Lukens JR, Eyo UB (2022) Microglia and neurodevelopmental disorders. *Annu Rev Neurosci* 45:425–445.
- Ma Z, et al. (2022) Deficiency of autism-related Scn2a gene in mice disrupts sleep patterns and circadian rhythms. *Neurobiol Dis* 168:105690.
- Mason ER, Soni DM, Chu S (2023) Microglial phagocytosis/cell health high-content assay. *Curr Protoc* 3:e724.
- McQuade A, Blurton-Jones M (2021) Human induced pluripotent stem cell-derived microglia (hiPSC-microglia). In: *Induced Pluripotent Stem (iPS) Cells: Methods and Protocols* (Nagy A, Turksen K, eds), pp 473–482. Ontario, Canada: Springer.
- McQuade A, Coburn M, Tu CH, Hasselmann J, Davtyan H, Blurton-Jones M (2018) Development and validation of a simplified method to generate human microglia from pluripotent stem cells. *Mol Neurodegener* 13:67.
- Meents JE, et al. (2019) The role of Nav1.7 in human nociceptors: insights from human induced pluripotent stem cell-derived sensory neurons of erythromelalgia patients. *Pain* 160:1327–1341.
- Merlini M, et al. (2021) Microglial Gi-dependent dynamics regulate brain network hyperexcitability. *Nat Neurosci* 24:19–23.
- Milescu LS, Bean BP, Smith JC (2010) Isolation of somatic Na⁺ currents by selective inactivation of axonal channels with a voltage prepulse. *J Neurosci* 30:7740–7748.
- Motipally SI, Allen KM, Williamson DK, Marsat G (2019) Differences in sodium channel densities in the apical dendrites of pyramidal cells of the electrosensory lateral line lobe. *Front Neural Circuits* 13:41.
- Nebeling FC, Poll S, Justus LC, Steffen J, Keppler K, Mittag M, Fuhrmann M (2023) Microglial motility is modulated by neuronal activity and correlates with dendritic spine plasticity in the hippocampus of awake mice. *Elife* 12:e83176.
- Olson JK, Miller SD (2004) Microglia initiate central nervous system innate and adaptive immune responses through multiple TLRs. *J Immunol* 173:3916–3924.
- Oyler J, Maljevic S, Scheffer IE, Berkovic SF, Petrou S, Reid CA (2018) Ion channels in genetic epilepsy: from genes and mechanisms to disease-targeted therapies. *Pharmacol Rev* 70:142–173.
- Paolicelli RC, et al. (2011) Synaptic pruning by microglia is necessary for normal brain development. *Science* 333:1456–1458.
- Pocock JM, Kettenmann H (2007) Neurotransmitter receptors on microglia. *Trends Neurosci* 30:527–535.
- Qu G, et al. (2024) Targeted blockade of aberrant sodium current in a stem cell-derived neuron model of SCN3A encephalopathy. *Brain* 147:1247–1263.
- Que Z, et al. (2021) Hyperexcitability and pharmacological responsiveness of cortical neurons derived from human iPSCs carrying epilepsy-associated sodium channel Nav1.2-L1342P genetic variant. *J Neurosci* 41:10194–10208.
- Sabate-Soler S, et al. (2022) Microglia integration into human midbrain organoids leads to increased neuronal maturation and functionality. *Glia* 70:1267–1288.
- Schafer DP, Lehrman EK, Kautzman AG, Koyama R, Mardinly AR, Yamasaki R, Ransohoff RM, Greenberg ME, Barres BA, Stevens B (2012) Microglia sculpt postnatal neural circuits in an activity and complement-dependent manner. *Neuron* 74:691–705.
- Schindelin J, et al. (2012) Fiji: an open-source platform for biological-image analysis. *Nat Methods* 9:676–682.
- Speicher AM, Wiendl H, Meuth SG, Pawlowski M (2019) Generating microglia from human pluripotent stem cells: novel in vitro models for the study of neurodegeneration. *Mol Neurodegener* 14:46.
- Sun Y, et al. (2016) A deleterious Nav1.1 mutation selectively impairs telencephalic inhibitory neurons derived from Dravet syndrome patients. *Elife* 5:e13073.
- Sun H, Li X, Guo Q, Liu S (2022) Research progress on oxidative stress regulating different types of neuronal death caused by epileptic seizures. *Neuro Sci* 43:6279–6298.
- Tidball AM, et al. (2020) Variant-specific changes in persistent or resurgent sodium current in SCN8A-related epilepsy patient-derived neurons. *Brain* 143:3025–3040.
- Umpierre AD, et al. (2023) Microglial P2Y6 calcium signaling promotes phagocytosis and shapes neuroimmune responses in epileptogenesis. *BioRxiv*.
- Umpierre AD, Bystrom LL, Ying Y, Liu YU, Worrell G, Wu L-J (2020) Microglial calcium signaling is attuned to neuronal activity in awake mice. *Elife* 9:e56502.
- Vahsen BF, et al. (2022) Human iPSC co-culture model to investigate the interaction between microglia and motor neurons. *Sci Rep* 12:12606.
- Vezzani A, Friedman A, Dingledine RJ (2013) The role of inflammation in epileptogenesis. *Neuropharmacology* 69:16–24.
- Weinhard L, et al. (2018) Microglia remodel synapses by presynaptic trogocytosis and spine head filopodia induction. *Nat Commun* 9:1228.
- Whitney R, Sharma S, Ramachandranair R (2023) Sudden unexpected death in epilepsy in children. *Dev Med Child Neurol* 65:1150–1156.
- Wolff M, et al. (2017) Genetic and phenotypic heterogeneity suggest therapeutic implications in SCN2A-related disorders. *Brain* 140:1316–1336.
- Wu W, Li Y, Wei Y, Bosco DB, Xie M, Zhao M-G, Richardson JR, Wu L-J (2020) Microglial depletion aggravates the severity of acute and chronic seizures in mice. *Brain Behav Immun* 89:245–255.
- Wu J, et al. (2024) Microglial over-pruning of synapses during development in autism-associated SCN2A-deficient mice and human cerebral organoids. *Mol Psychiatry* 29:2424–2437.
- Wyatt-Johnson SK, Herr SA, Brewster AL (2017) Status epilepticus triggers time-dependent alterations in microglia abundance and morphological phenotypes in the hippocampus. *Front Neurol* 8:700.
- Xie Y, Ng NN, Safrina OS, Ramos CM, Ess KC, Schwartz PH, Smith MA, O'Dowd DK (2020) Comparisons of dual isogenic human iPSC pairs identify functional alterations directly caused by an epilepsy associated SCN1A mutation. *Neurobiol Dis* 134:104627.
- Yang X-R, Ginjupalli VKM, Theriault O, Poulin H, Appendino JP, Au PYB, Chahine M (2022) SCN2A-related epilepsy of infancy with migrating

- focal seizures: report of a variant with apparent gain-and loss-of-function effects. *J Neurophysiol* 127:1388–1397.
- Yokoi T, Enomoto Y, Tsurusaki Y, Naruto T, Kurosawa K (2018) Nonsyndromic intellectual disability with novel heterozygous SCN2A mutation and epilepsy. *Hum Genome Var* 5:20.
- Zeng Q, et al. (2022) SCN2A-related epilepsy: the phenotypic spectrum, treatment and prognosis. *Front Mol Neurosci* 15:1–12.
- Zhang J, et al. (2021) Severe deficiency of the voltage-gated sodium channel NaV1. 2 elevates neuronal excitability in adult mice. *Cell Rep* 36:109495.
- Zhang X, Wang D, Zhang B, Zhu J, Zhou Z, Cui L (2020) Regulation of microglia by glutamate and its signal pathway in neurodegenerative diseases. *Drug Discov Today* 25:1074–1085.
- Zhao HW, Gu XQ, Chailangkarn T, Perkins G, Callacondo D, Appenzeller O, Poulsen O, Zhou D, Muotri AR, Haddad GG (2015) Altered iPSC-derived neurons' sodium channel properties in subjects with Monge's disease. *Neuroscience* 288:187–199.
- Zhao S, Wang L, Liang Y, Zheng J, Umpierre AD, Wu L-J (2024) Chemogenetic activation of microglial Gi signaling decreases microglial surveillance and impairs neuronal synchronization. *bioRxiv*, 2024.2002. 2012.579861.